

Formation of super-massive black holes in galactic nuclei I: delivering seed intermediate-mass black holes in massive stellar clusters

Abbas Askar,¹★ Melvyn B. Davies¹ and Ross P. Church¹

¹Lund Observatory, Department of Astronomy, and Theoretical Physics, Lund University, Box 43, SE-221 00 Lund, Sweden

Accepted 2021 January 12. Received 2021 January 12; in original form 2020 June 08

ABSTRACT

Supermassive black holes (SMBHs) are found in most galactic nuclei. A significant fraction of these nuclei also contain a nuclear stellar cluster (NSC) surrounding the SMBH. In this paper, we consider the idea that the NSC forms first, from the merger of several stellar clusters that may contain intermediate-mass black holes (IMBHs). These IMBHs can subsequently grow in the NSC and form an SMBH. We carry out N -body simulations of the simultaneous merger of three stellar clusters to form an NSC, and investigate the outcome of simulated runs containing zero, one, two and three IMBHs. We find that IMBHs can efficiently sink to the centre of the merged cluster. If multiple merging clusters contain an IMBH, we find that an IMBH binary is likely to form and subsequently merge by gravitational wave emission. We show that these mergers are catalyzed by dynamical interactions with surrounding stars, which systematically harden the binary and increase its orbital eccentricity. The seed SMBH will be ejected from the NSC by the recoil kick produced when two IMBHs merge, if their mass ratio $q \gtrsim 0.15$. If the seed is ejected then no SMBH will form in the NSC. This is a natural pathway to explain those galactic nuclei that contain an NSC but apparently lack an SMBH, such as M33. However, if an IMBH is retained then it can seed the growth of an SMBH through gas accretion and tidal disruption of stars.

Key words: stars: black holes – galaxies: star clusters: general – (galaxies:) quasars: super-massive black holes – gravitational waves – methods: numerical

1 INTRODUCTION

The nuclei of most galaxies with stellar masses larger than $10^8 M_\odot$ contain either a nuclear star cluster (NSC), a supermassive black hole (SMBH), or both. NSCs are massive and dense stellar clusters that reside in the nuclei of their host galaxies. They typically have effective radii of a few parsecs with central densities of up to $10^7 M_\odot \text{pc}^{-3}$ (Georgiev et al. 2016; Schödel et al. 2018). About 80 per cent of galaxies of all morphological types that have stellar masses in the range 10^8 to $10^{10} M_\odot$ harbour an NSC (see Neumayer et al. 2020, and references therein). In many galaxies, including the Milky Way and M31, an NSC coexists with an SMBH (Seth et al. 2008; Neumayer & Walcher 2012; Neumayer et al. 2020). Some galaxies however, such as M33, contain an NSC (Kormendy & McClure 1993; Gordon et al. 1999) but show no evidence for the presence of an SMBH in their nuclei (Merritt et al. 2001; Gebhardt et al. 2001). Typically, elliptical galaxies with stellar masses greater than $10^{11} M_\odot$ have low nucleation fractions and contain only an SMBH at their centre (Côté et al. 2006; Graham & Spitler 2009; Seth et al. 2020). Both NSCs and SMBHs follow tight cor-

relations with the properties of their host galaxies (Ferrarese et al. 2006; Leigh et al. 2015; Capuzzo-Dolcetta & Tosta e Melo 2017) and this suggests that the formation and subsequent growth of both NSCs and SMBHs could be closely related (Antonini et al. 2015; Neumayer et al. 2020).

Two main scenarios for the formation of NSCs have been proposed. NSCs may have formed from the merger of infalling stellar clusters that aggregate to the galactic centre due to dynamical friction (Tremaine et al. 1975; Capuzzo-Dolcetta 1993; Lotz et al. 2001; Oh & Lin 2000; Agarwal & Milosavljević 2011; Tsatsi et al. 2017) or they may have formed through in-situ star formation triggered by high gas densities in the galactic nuclei (Loose et al. 1982; Mihos & Hernquist 1994; Milosavljević 2004; Nayakshin et al. 2007; Aharon & Perets 2015). Observations of NSCs show that they contain stars with diverse ages and metallicities and it is likely that both cluster infall and in-situ star formation contribute to the growth of NSCs (Antonini et al. 2015; Guillard et al. 2016; Neumayer et al. 2020; Do et al. 2020; Arca Sedda et al. 2020a).

SMBHs have masses in the range $10^6 - 10^{10} M_\odot$ and their formation and growth remains an open question (Latif & Ferrara 2016). It is likely that SMBHs grew from smaller seed black holes (BHs), however, the exact seeding mechanism and the masses of

★ E-mail: askar@astro.lu.se (AA)

these seed BHs are not known. These seed BHs could have originated from the evolution of massive stars or they may have formed with large initial masses of the order $10^5 M_\odot$ (Volonteri 2010; Johnson et al. 2013; Greene et al. 2019). In the former case, BHs with masses in the intermediate-mass range of $10^2 - 10^5 M_\odot$ ought to have existed in order to seed SMBHs. It has been postulated that such intermediate-mass BHs (IMBHs) could form through dynamical processes in dense stellar clusters such as globular clusters or young massive clusters (see Section 3.1). Due to uncertainties in their formation mechanism, it is not clear which forms first, the NSC or an SMBH. If an SMBH grows from lower-mass seed BHs in dense environments then it is possible that the formation of an NSC precedes the formation of an SMBH (Devecchi & Volonteri 2009; Davies et al. 2011; Miller & Davies 2012; Neumayer & Walcher 2012; Gnedin et al. 2014).

Given that an NSC may form due to the inspiral and merger of smaller stellar clusters, it is likely that some of the merging clusters may already have formed a seed IMBH, which could then be delivered to the NSC (Ebisuzaki et al. 2001; Kim et al. 2004; Portegies Zwart et al. 2006; Devecchi et al. 2012; Petts & Gualandris 2017; Davies et al. 2020). Once an IMBH is delivered to the NSC, it can become a seed SMBH and continue to grow through tidal captures/disruption of stars (Stone et al. 2017; Alexander & Bar-Or 2017; Boekholt et al. 2018; Arca-Sedda & Capuzzo-Dolcetta 2019) or through continued gas accretion which can also contribute to the growth of the NSC (Devecchi & Volonteri 2009; Davies et al. 2011; Guillard et al. 2016; Pacucci et al. 2017; Natarajan 2020; Das et al. 2020). In the latter case, a seed IMBH of $10^4 M_\odot$ can grow up to $10^9 M_\odot$, if it is able to accrete at the Eddington rate for 500 Myr (Madau et al. 2014). BHs can grow rapidly if they have low spin values following episodes of chaotic accretion (King & Pringle 2006; King et al. 2008). It is also likely that multiple IMBHs are delivered to the growing NSC from more merging clusters (Ebisuzaki et al. 2001; Mastrobuono-Battisti et al. 2014). This may result in the formation of a binary IMBH which could merge by emitting gravitational waves (Amaro-Seoane & Freitag 2006; Tamfal et al. 2018; Rasskazov et al. 2019; Arca Sedda & Mastrobuono-Battisti 2019; Wirth & Bekki 2020). Provided that the gravitational wave (GW) recoil kick from the merger of two IMBHs is less than the escape speed of the NSC, the merged IMBH can be retained in the NSC and can grow into an SMBH (Amaro-Seoane & Freitag 2006; Gürkan et al. 2006; Amaro-Seoane et al. 2007, 2017; Arca Sedda & Mastrobuono-Battisti 2019). However, if the gravitational recoil kick is larger than the escape speed of the cluster then the merged IMBH will be ejected from the NSC and the seed SMBH will be lost. Dynamical ejection of one or more IMBHs can also occur through binary-single encounters involving three IMBHs. Therefore, these interactions could also potentially remove a seed SMBH from an NSC.

Several studies have numerically investigated the formation of an NSC by merging stellar clusters. Hartmann et al. (2011) carried out collisionless N -body simulations of stellar clusters merging at the centre of a galactic disc to form an NSC that had properties comparable to observed NSCs. Miocchi et al. (2006); Capuzzo-Dolcetta & Miocchi (2008) carried out simulations of clusters infalling in a galactic centre and showed that they can survive strong tidal interactions and merge to form dense NSCs. Antonini et al. (2012) carried out N -body simulations to follow the successive inspiral and merger of twelve globular clusters in an initial setup which included a low-density nuclear stellar disc and an SMBH similar in mass to Sagittarius A*. They found that the NSC produced from these merging clusters had properties similar to those of the Milky

Way NSC, and concluded that nearly half of the stars in the Milky Way NSC originated from merging clusters while the rest probably formed in-situ. Mastrobuono-Battisti et al. (2014) used the same initial set-up as Antonini et al. (2012) but included IMBHs at the centre of their merging clusters. They found that the IMBHs inspiral to the core of the NSC where they interact with surrounding stars and each other. The inclusion of IMBHs shortens the relaxation time of the NSC and also increases the rate of tidal disruption events. Arca-Sedda et al. (2015) also carried out simulations of merging stellar clusters with the goal to model the future evolution of the galactic nucleus in Henize 2–10. With the exception of one run, they also had an existing SMBH in their galactic nuclei. They found that an NSC forms in all their models and in the simulated run without an SMBH, the most massive infalling clusters lose less mass as they decay towards the galactic centre. Arca-Sedda & Capuzzo-Dolcetta (2017) used N -body simulations to investigate the role of galaxy structure in determining the density distribution of an NSC and its implications for SMBH seeding.

Semi-analytical models have also been developed to investigate the formation of NSCs through mergers of globular clusters that undergo dynamical friction (Antonini 2013; Gnedin et al. 2014; Arca-Sedda & Capuzzo-Dolcetta 2014). The results from these models are able to reproduce some of the observed properties of NSCs (Neumayer et al. 2020). Using models for galaxy formation that included prescriptions for NSC formation and dynamical heating from massive BHs, Antonini et al. (2015) were able to account for low nucleation fractions in massive elliptical galaxies (Neumayer & Walcher 2012; Arca-Sedda et al. 2016).

In this work, we focus on the formation of an NSC through mergers of stellar clusters. We carry out several N -body simulations to follow the final stages of an idealized merger of three stellar clusters with no existing SMBH. Firstly, we merge clusters that only contain stars (Section 2); then we include various combinations of IMBHs at the centre of the merging clusters to investigate how IMBHs would evolve within the merged cluster. In Section 3, we describe runs in which there is a single IMBH in the three merging clusters and also discuss various mechanisms by which IMBHs can form in dense star clusters (Section 3.1). In Sections 4 and 5, we present results from runs in which the initial set-up contains two and three IMBHs. We find that in these runs, we can form a binary IMBH that hardens and becomes more eccentric as it interacts with surrounding stars (Quinlan & Shapiro 1990; Sesana et al. 2006; Baumgardt et al. 2006; Iwasawa et al. 2011). By reaching high orbital eccentricities, these binaries can efficiently merge due to GW emission within several hundred Myr. The evolution of the orbital parameters of these binaries are discussed in Appendix A.

In Section 6, we describe important processes such as GW recoil kicks (Section 6.1) and strong scattering encounters (Section 6.2) between IMBHs that can influence the retention of seed SMBHs in NSCs. We argue that there are two routes that endow galaxies with an NSC but no SMBH. Firstly, they may never have had a seed IMBH; i.e. none of the clusters that combine to form the NSC contained an IMBH. The second possibility is that the seed SMBH may have been ejected whilst it was still growing. If an IMBH is retained or already exists in an NSC, then it can grow to become an SMBH. In a subsequent paper, we use the results presented here to model the retention and growth of seed SMBHs in a population of galaxies where the NSC is constructed through the merger of stellar clusters.

2 SIMULATING MERGING STELLAR CLUSTERS

We simulate the final stages of an idealized merger of three stellar clusters to form an NSC. In Section 2.1, we describe the details of our simulation set-up for three merging clusters and briefly describe how these clusters evolve in Section 2.2. In the runs presented in this paper, there is no existing SMBH and there is no galactic tidal field.

2.1 N-body simulations: Set-up and Initial Conditions

We use a series of direct N -body simulations of the merger of three stellar clusters. We consider a range of cases where various combinations of the three merging clusters initially contain an IMBH at their centre. The simulations were carried out using the NBODY6++GPU (Wang et al. 2015) code. This is an extension of the well-known NBODY6 code developed by Aarseth (1999); Aarseth (2003) and its GPU accelerated version NBODY6GPU code (Nitadori & Aarseth 2012) for simulating star cluster evolution.

NBODY6++GPU uses the fourth-order Hermite integration method together with hierarchical block time steps. In order to speed up force calculations, the code uses Ahmad & Cohen (1973) neighbor scheme that separates integration of regular and irregular forces using large time-steps and small time-steps respectively. NBODY6++GPU combines GPU acceleration with MPI parallelization so that the code maybe used across multiple nodes on computer clusters. The code can accurately treat binary systems and close encounters through the Kustaanheimo & Stiefel (1965) and chain regularization (Mikkola & Aarseth 1993) algorithms. It also contains prescriptions for stellar and binary evolution based on the SSE and BSE codes (Hurley et al. 2000, 2002).

Using NBODY6++GPU we generated three initial models for stellar clusters comprising 50 000, 30 000 and 15 000 particles. Each of these was a Plummer model consisting of single stars with masses between 0.5 and 2 M_{\odot} . Within this range, the zero-age-main sequence (ZAMS) masses were sampled using a power law initial mass function with $\alpha = 2.3$ (Kroupa 2001). Initial ZAMS radii for the stars were generated for a metallicity of $Z = 0.001$ ($[\text{Fe}/\text{H}] = -1.301$). The initial half-mass radii of the clusters were 2.4 pc with a Plummer scale length of 1.82 pc. Table 1 contains the properties of the three modelled clusters. For each of the three stellar clusters, we also generated models that, in addition to stars, contained a central IMBH of 1000, 500, 200, or 100 M_{\odot} .

Using these three initial models, we set-up an initial model which is meant to represent the final stage of the merger of three stellar clusters. We place the cluster with 50 000 particles in the centre, the cluster with 30 000 particles is offset in the X direction by 20 pc from the centre, and the cluster with 15 000 particles is offset in the X direction by -20 pc. In order to place the clusters with 30 000 particles and 15 000 particles on sub-circular orbits around the central cluster, we added offsets to the Y component of the initial velocities of -2.8 and 1.4 km s^{-1} respectively. Fig. 1 is a particle plot showing the initial $X - Y$ positions of the three clusters in a coordinate system centred on the global centre of mass. The two 30 000 and 15 000 particle clusters were placed sufficiently close to the central cluster so that they both fill their Roche-lobe and merge with the central cluster on a dynamical timescale. While the number of stars and the total stellar mass in these merging clusters is smaller than typical NSCs, the approach taken in this work allows us to capture IMBH dynamics and the effect of close encounters involving stellar mass stars on IMBH binary evolution.

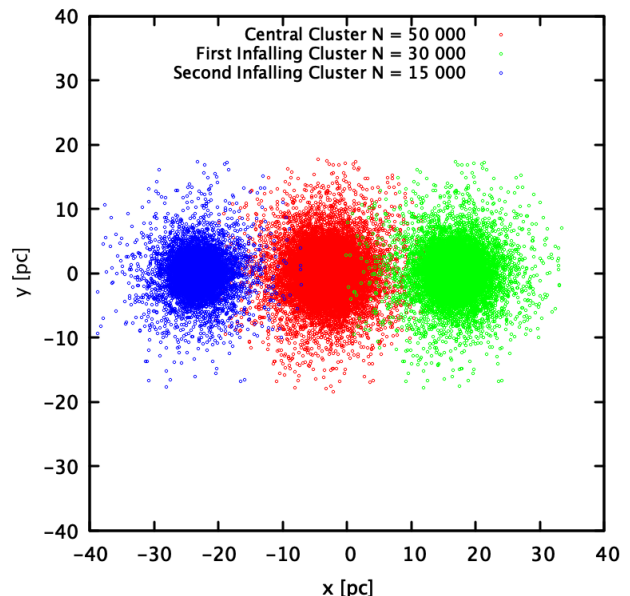


Figure 1. $X - Y$ particle plot showing the initial set-up for the three merging clusters described in Section 2.1. The origin is centred on the global centre of mass. Red particles are stars that belong to the cluster placed in the middle with 50 000 stars, the green particles belong to the cluster with 30 000 stars which is offset in the X direction from the centre of the central cluster by 20 pc and the blue particles belong to the cluster with 15 000 stars which is offset in the X direction by -20 pc.

This is particularly important for the results of the runs presented in Section 4 and 5.

In this section, we present a run where the merging clusters contain only stars. We then add IMBHs to this initial set-up in order to differentially measure the effects of IMBH inclusion. In Section 3, we describe the runs with one IMBH. In Sections 4 and 5, we describe runs that contain two and three IMBHs. The runs have been named in the format $X.i$, where X indicates the number of IMBHs in that run and i is the run number. So 0.1, is the run which contains no IMBH, 1.2 is the second run with initially one IMBH. In total we have eleven simulations comprising one run with no IMBH (0.1), three runs with one IMBH (1.i), four runs with two IMBHs (2.i), and three runs with three IMBHs (3.i).

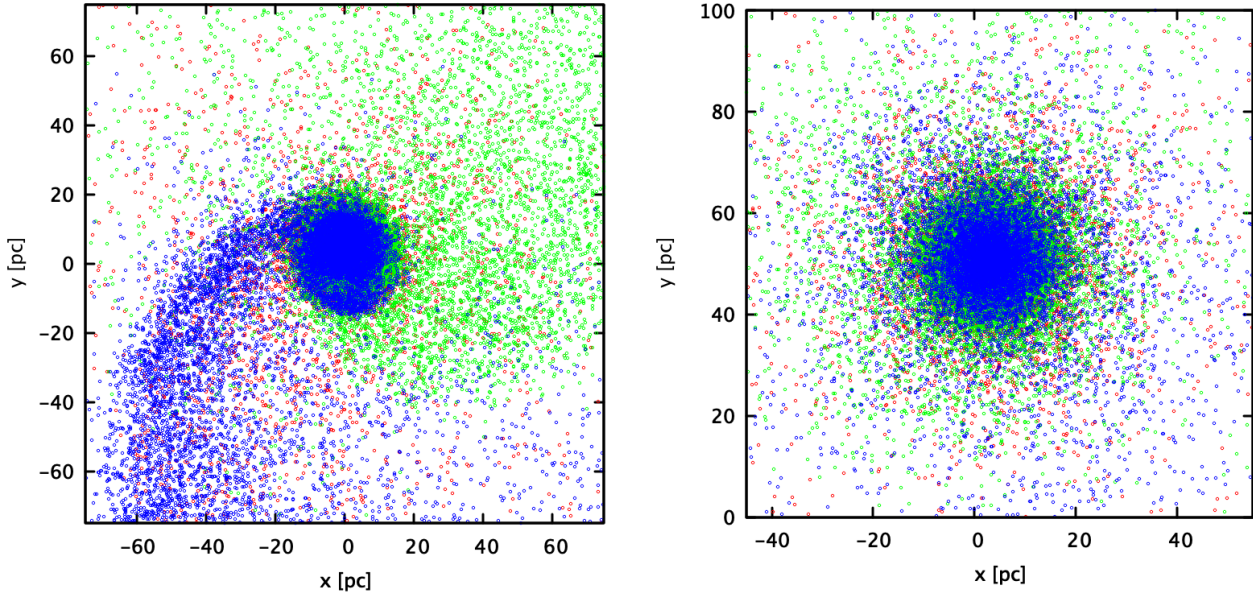
2.2 Evolution of merging clusters without IMBHs

Within the first few time steps, the two infalling clusters begin to merge into the central cluster. As the merger proceeds, the infalling clusters produce large tidal tails of stars, some of which gradually return and fall in to the central cluster. We simulated the model up to 375 Myr, by which time all the three clusters had merged into a single cluster with a dense core. In Fig. 2, we show particle plots at 28.8 Myr and 360 Myr. At 28.8 Myr, the tidal tails of stars from the infalling star clusters with 30 000 and 15 000 stars can be seen in green and blue respectively. At 360 Myr, we find that the final merged cluster now has a core containing stars from all the three merged clusters and there are no visible tidal tails in the vicinity of the cluster.

In Fig. 3, we compare the density profile of the merged cluster

Table 1. In this table, the initial properties of the three individual merging clusters are provided

Model	Number	Initial Mass [M_{\odot}]	Half-mass Radius [pc]	Plummer Scale Radius [pc]	Half-Mass Relaxation Time [Myr]
Central	5.0×10^4	4.42×10^4	2.40	1.84	160
First Infalling	3.0×10^4	2.65×10^4	2.40	1.84	130
Second Infalling	1.5×10^4	1.33×10^4	2.40	1.84	99

**Figure 2.** Particle plots in the $X - Y$ plane for model 0.1, which contains no IMBHs. The different colours represent stars from the three initial clusters as shown in Fig. 1. The left panel shows the clusters spiralling together at 28.8 Myr. The right panel shows the resulting single, merged cluster at 360 Myr. The core of the cluster appears blue owing to a plotting artefact: the core is a mixture of stars from all the three stellar clusters.

at 360 Myr to the initial density profiles of the three individual merging clusters in Fig. 3. The merged cluster at 360 Myr has a slightly larger central density than the initial clusters. This increase in density of the merged cluster due to gravitational encounters is also reported by Antonini et al. (2012) and Mastrobuono-Battisti et al. (2019).

3 MERGING STAR CLUSTERS WITH ONE IMBH

3.1 IMBH formation in star clusters

It has been hypothesized that IMBHs of $10^2 - 10^4 M_{\odot}$ may form in the dense environments of stellar clusters (see Greene et al. 2019, and references therein), either through runaway mergers of massive stars that may lead to the formation of a seed IMBH (Portegies Zwart & McMillan 2002; Freitag et al. 2006; Giersz et al. 2015; Mapelli 2016; Gieles et al. 2018; Reinoso et al. 2018; Tagawa et al. 2020), or through the gradual growth of stellar-mass BHs via mergers with other BHs or stars (Miller & Hamilton 2002; Giersz et al. 2015; Haster et al. 2016; Rizzuto et al. 2020). Seed BHs of $10^2 - 10^3 M_{\odot}$ can grow to larger masses through tidal capture and disruption events in dense clusters (Stone et al. 2017; Alexander & Bar-Or 2017; Sakurai et al. 2019). Moreover, stellar-mass seed BHs can also grow by accretion of gas in primordial, gas-rich, massive stellar clusters (Vesperini et al. 2010; Leigh et al. 2013). Observa-

tionally, identifying the presence of an IMBH in a stellar cluster is challenging (Noyola et al. 2008; Mezcua 2017; de Vita et al. 2017; Zocchi et al. 2019; Aros et al. 2020) and kinematic studies searching for the presence of IMBHs in Galactic globular clusters have yielded inconclusive results (Lützendorf et al. 2013a; Lanzoni et al. 2013; Kızıltan et al. 2017; Mann et al. 2019; Baumgardt et al. 2019). Searching for accretion signatures of an IMBH in Galactic globular clusters using radio observations has also not found any evidence for IMBHs (Strader et al. 2012; Tremou et al. 2018). Lin et al. (2018) identified an IMBH candidate in an extragalactic massive star cluster through an X-ray flare that originated from a tidal disruption event (Lin et al. 2020). Additionally, a few low mass SMBHs have also been observed in galactic nuclei. Baldassare et al. (2015), used optical and X-ray observations to identify a BH with a mass of $5 \times 10^4 M_{\odot}$ in the dwarf galaxy RGG 118. Nguyen et al. (2019) constrained the mass of a BH at the centre of the dwarf elliptical galaxy NGC 205 to be less than $7 \times 10^4 M_{\odot}$. Recent observations of molecular gas streams in the Galactic centre have also identified possible IMBH candidates (Takekawa et al. 2019, 2020). The detection of gravitational waves from the merger of an $\sim 85 M_{\odot}$ and a $\sim 66 M_{\odot}$ BH (GW190521) by the LIGO/Virgo collaboration (Abbott et al. 2020) resulted in the formation of a $\sim 142 M_{\odot}$ BH. This is the first clear detection of a low-mass IMBH and it has been suggested that such massive merging binary BHs can form in star clusters (Di Carlo et al. 2020; Samsing & Hotokezaka 2020; Fra-

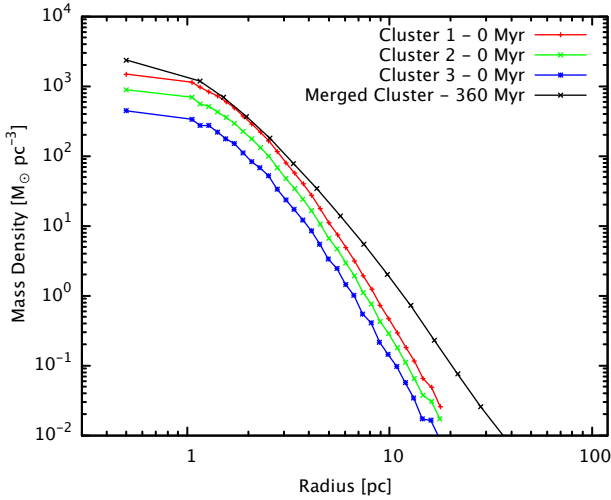


Figure 3. Density profiles for the three merging clusters at $t = 0$ and the merged cluster at 360 Myr (black line). The red coloured line shows the initial density profile for the central cluster with 50 000 stars, the green line corresponds to the more massive infalling cluster that contains 30 000 stars, and the blue line corresponds to the cluster with 15 000 stars. The merged cluster at 360 Myr is more radially extended and has a denser core than the three initial merging clusters.

gione et al. 2020; Martinez et al. 2020; Kremer et al. 2020; Arca Sedda et al. 2020b; Romero-Shaw et al. 2020).

Monte Carlo simulations of globular cluster models by Giersz et al. (2015) using the *MOCCA* code (Hypki & Giersz 2013; Giersz et al. 2013) showed that an IMBH may grow in a globular cluster through direct collisions and dynamical interactions between a BH and other objects. In Giersz et al. (2015), two scenarios for IMBH formation are described, the “fast” and “slow” scenarios. In the fast scenario, an IMBH of $10^2 - 10^4 M_\odot$ forms in initially dense globular cluster models – those with central densities of $\gtrsim 10^7 M_\odot \text{pc}^{-3}$. In a significant fraction of these simulations, the IMBH formation occurs within tens of Myr due to runaway mergers between massive main-sequence stars (Quinlan & Shapiro 1990; Lee 1993; Portegies Zwart & McMillan 2002) leading to the formation of a massive star which absorbs a stellar-mass BH (Rizzuto et al. 2020). These models assume that all of the mass of the main-sequence star is transferred to the BH in such mergers, facilitating the formation of the seed IMBH. Additional simulations from Giersz et al. (2015) in which only 25 per cent of the main sequence star mass is accreted by the BH in the case of such mergers also lead to the formation of an IMBH. In the “slow” scenario, a stellar-mass BH grows gradually through mergers with other BHs or through tidal disruption of stars during core collapse. In these models, the core collapse occurs after few to several Gyr of cluster evolution in models that are initially not too dense (Arca Sedda et al. 2019a). The fraction of these simulated models that form an IMBH with a mass of at least $100 M_\odot$ correlates with the initial mass of the cluster. About 20 per cent of clusters with an initial mass of around $10^5 M_\odot$ form an IMBH. This fraction increases to about 50 per cent for models with an initial mass of around $10^6 M_\odot$.

In Fig. 4, we show the evolution of the most massive BHs in *MOCCA* simulations of stellar cluster models that formed a BH larger than $100 M_\odot$. These models had initially 10^5 stellar systems (binary systems + single stars) and different initial parameters. Details of the initial model set-up for the *MOCCA*-Survey Database I can be found

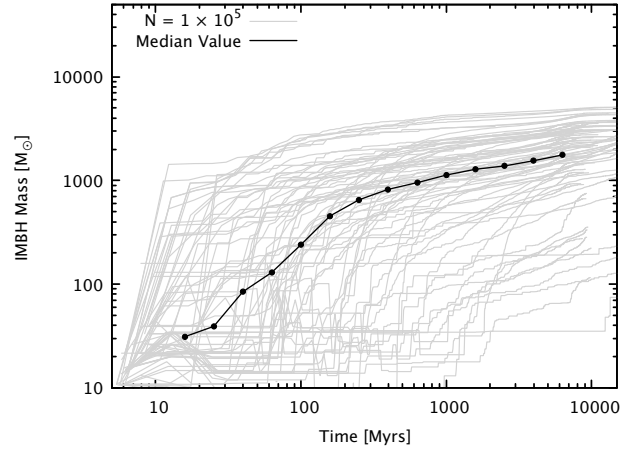


Figure 4. Masses of IMBHs as functions of time produced in clusters initially containing 1.0×10^5 stars. The results are taken from the Monte-Carlo N -body code *MOCCA* and the *MOCCA*-Survey Database I project (Askar et al. 2017). Each grey line represents a different simulation. The black line shows the median IMBH mass over the model set.

Table 2. In this table we describe the runs that contain one IMBH. The first column contains an identifier for the run, the second column contains the time up to which the simulation was run in Myr. The third column contains the total mass of the merging clusters. Columns 4 to 6 give the IMBH mass in the run and also describe the position of the IMBH in the initial set-up. IMBH₁ indicates that the IMBH was initially at the centre of the cluster with 50 000 stars, IMBH₂ is initially at the centre of the cluster with 30 000 stars, and IMBH₃ is at the centre of the cluster with 15 000 stars. Column 7 gives the time it takes the BH to sink to the central part of the merged cluster (within 0.25 pc from the centre of mass).

Run	Time [Myr]	Total Mass [M_\odot]	IMBH ₁ [M_\odot]	IMBH ₂ [M_\odot]	IMBH ₃ [M_\odot]	t_{sink} [Myr]
1.1	250	8.50×10^4	1000	0	0	35
1.2	357	8.45×10^4	0	500	0	61
1.3	551	8.42×10^4	0	0	200	48

in Askar et al. (2017). The median IMBH mass in these clusters after 100 Myr of evolution is a few hundred solar masses. The number of stars and the total mass in these simulations depend the initial binary fraction which varied between 5 and 95 per cent. The initial masses of the clusters plotted in 4 are between $5.85 - 9.12 \times 10^4 M_\odot$. For these models, the IMF is sampled between 0.08 and $100 M_\odot$.

3.2 Merging clusters that contain 1 IMBH (1.i runs)

We simulated three runs which had the same set-up as the run described in Section 2.2, but with an IMBH in the centre of one of the merging clusters. The IMBH mass and the cluster to which we added it are described in Table 2. In these runs, the IMBH mass was taken to be a reasonable fraction of the total cluster mass. We consider IMBHs of $1000 M_\odot$, $500 M_\odot$ and $200 M_\odot$ that are consistent with IMBH masses after few hundred Myr in *MOCCA* simulations with initially 40 000 to 10^5 objects (Arca Sedda et al. 2019a).

We find that runs 1.1, 1.2 and 1.3 evolve in a similar way to run 0.1. Since the mass of the IMBH in run 1.i is much smaller than the total mass of the merging clusters, presence of the IMBH does

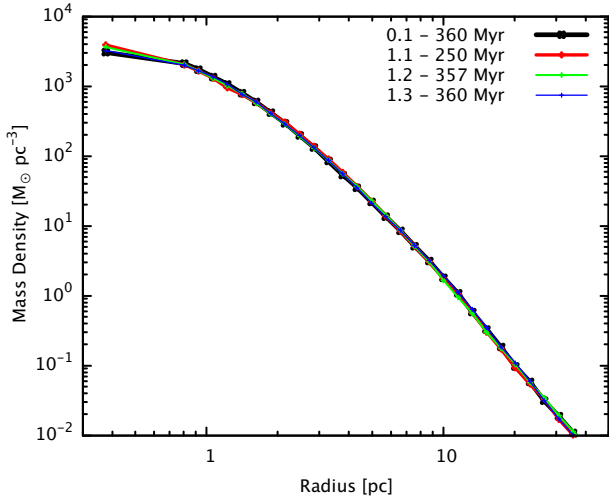


Figure 5. Mass density profiles for the merged clusters in runs 1.1 (red), 1.2 (green) and 1.3 (blue) and run 0.1 (black). The profiles were plotted at about 360 Myr from the start of the simulation for runs 1.2, 1.3 and 0.1. For cluster 1.1, the plot was made for the snapshot at 250 Myr (see Table 2). All the four merged clusters have a similar density profile.

not significantly affect the cluster evolution. Hence, the properties and appearance of the merged cluster are the same as run 0.1. To illustrate this, we show the mass density profile of runs 1.i and 0.1 in Fig. 5. For runs 0.1, 1.2 and 1.3, the profiles are plotted at about 360 Myr, while for run 1.1 the profile is shown for the last simulation snapshot at 250 Myr. The density profiles for the merged clusters in runs 1.i are similar and are also in agreement with run 0.1. The only differences are in the central density value which includes the IMBH mass.

In run 1.1, the IMBH was already at the centre of the most massive cluster that we placed in the middle while in runs 1.2 and 1.3 it was brought along with the two less massive infalling clusters. In all the runs, the IMBH ends up in the cluster centre due to mass segregation. It has been shown that the orbital decay time of the IMBH in an NSC depends on its mass and the density of surrounding stars (Arca-Sedda & Gualandris 2018). Since $M_\star \ll M_{\text{IMBH}}$ in our runs, dynamical friction is efficient at bringing the IMBHs to centre of the merged cluster. In run 1.2, the $500 M_\odot$ IMBH, that was initially at the centre of the infalling cluster with 30 000 stars, arrives at the centre of the merged cluster in about 20 Myr and settles within 0.25 pc from the centre of mass within 60 Myr. In run 1.3, a $200 M_\odot$ IMBH was placed at the centre of the infalling cluster with 15 000 stars and it arrives at the centre of the merging cluster in about 38 Myr and settles within 0.25 pc of the centre of mass within 50 Myr. These runs show that the IMBHs brought along by merging stellar clusters can effectively sink to the centre of an NSC within a few tens of Myr from the beginning of the cluster merger.

One of the underlying assumptions in these runs is that the individual star clusters had evolved for about 100 Myr before they merged with each other. This assumption has implications on the location where the clusters may have been born in order for them to effectively sink to the inner 20 pc of a galaxy on a timescale of about a 100 Myr and have had sufficient time to form an IMBH. There is observational evidence for the presence of young clusters with masses larger than $10^5 M_\odot$ in the innermost 150 pc of a few dwarf starburst galaxies and the inferred dynamical friction time for

Table 3. This table describes the four runs that contain two IMBHs. The description of the columns is the same as it was for Table 2. The runs have been labelled with the colours that are used for them in Figs. 6, 7, 12 and 15.

Run	Time [Myr]	Total Mass [M_\odot]	IMBH ₁ [M_\odot]	IMBH ₂ [M_\odot]	IMBH ₃ [M_\odot]
2.1 •	716	8.55×10^4	1000	500	0
2.2 •	914	8.50×10^4	1000	100	0
2.3 •	825	8.52×10^4	1000	200	0
2.4 •	745	8.47×10^4	0	500	200

these clusters is ~ 0.1 –1 Gyr (Nguyen et al. 2014; Antonini 2014; Arca-Sedda et al. 2015).

4 SIMULATIONS CONTAINING TWO IMBHs (2.I RUNS)

If NSCs are built up from multiple merging stellar clusters then it is possible that some of these clusters have formed IMBH in their centres through the mechanisms described in Section 3.1. In that case, multiple IMBHs may be delivered to the galactic nucleus by merging stellar clusters. To check how multiple IMBHs evolve within the merged clusters, we also carried out runs in which we placed two or three IMBHs at the centre of the merging clusters. The evolution of the runs containing two IMBHs are described in this Section.

Using the same initial setup for three merging clusters described in Section 2.1, we set-up four runs in which we placed IMBHs at the centre of two of the three merging clusters. In three of these runs (labelled 2.1 to 2.3), the central cluster with 50 000 particles contains an IMBH of $1000 M_\odot$ and the first infalling cluster, with 30 000 particles, contains IMBHs of masses $500 M_\odot$ (run 2.1), $100 M_\odot$ (run 2.2) and $200 M_\odot$ (run 2.3). In the run labelled 2.4, the central cluster does not contain an IMBH; instead, the infalling clusters with 30 000 and 15 000 particles contain IMBHs of $500 M_\odot$ and $200 M_\odot$ respectively. The set-up of these runs is summarised in Table 3.

The left panel in Fig. 6 shows the instantaneous separation of the two IMBHs as a function of time for the first 100 Myr. The non-smooth lines in the left panel are due to the orbital eccentricity of the binary IMBH system. For models labelled 2.1 to 2.3, the binary forms within 20–30 Myr. The model with the most massive secondary IMBH (2.1), segregates and finds the primary IMBH within 20 Myr and the model with the least massive secondary IMBH (2.2) takes slightly longer to form a binary system with the primary IMBH. For the model labelled 2.4, there was no central IMBH so the initial separation between the two IMBHs is about 40 pc. For this run, it takes the IMBHs about 100 Myr to form a close binary system.

The right panel in Fig. 6 shows the evolution of the mass enclosed between the two IMBHs as a function of time in the four 2.i runs. The enclosed mass is calculated by summing up the mass of stars that are enclosed within a sphere centred around the midpoint between the two IMBHs and its radius is given by the length of this midpoint between the two IMBHs. At the end of the lines in the right panel of Fig. 6, the IMBH binaries have evacuated all of the stars originally contained within their orbits by scattering them away (Makino & Funato 2004; Berczik et al. 2005; Merritt 2006).

We follow the evolution of the merging clusters for several hundred Myr. The long-term evolution of the semi-major axis and the orbital eccentricity of the binary IMBH in each of the 2.i runs

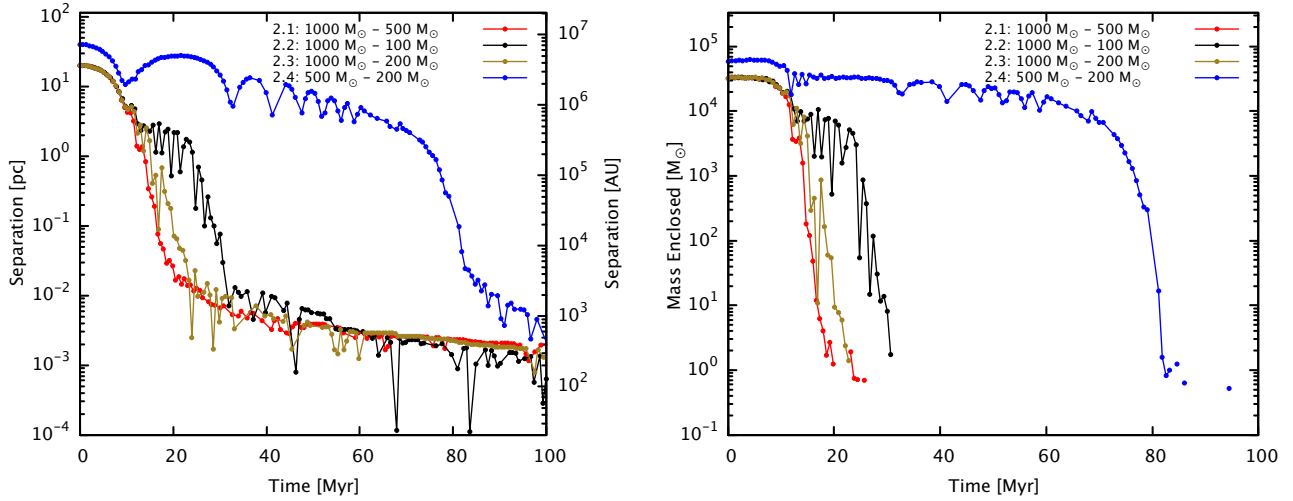


Figure 6. The left panel shows the instantaneous separation between the two IMBHs in the 2.i runs during the first 100 Myr. The red, black, olive and blue lines correspond to runs 2.1, 2.2, 2.3 and 2.4 respectively. The non smooth lines are due to orbital eccentricity of the binary IMBH. The right panel shows the evolution of the mass enclosed between the two IMBHs as functions of time in the four 2.i runs. At the ends of the lines the IMBH binaries have evacuated all of the stars originally contained within their orbits.

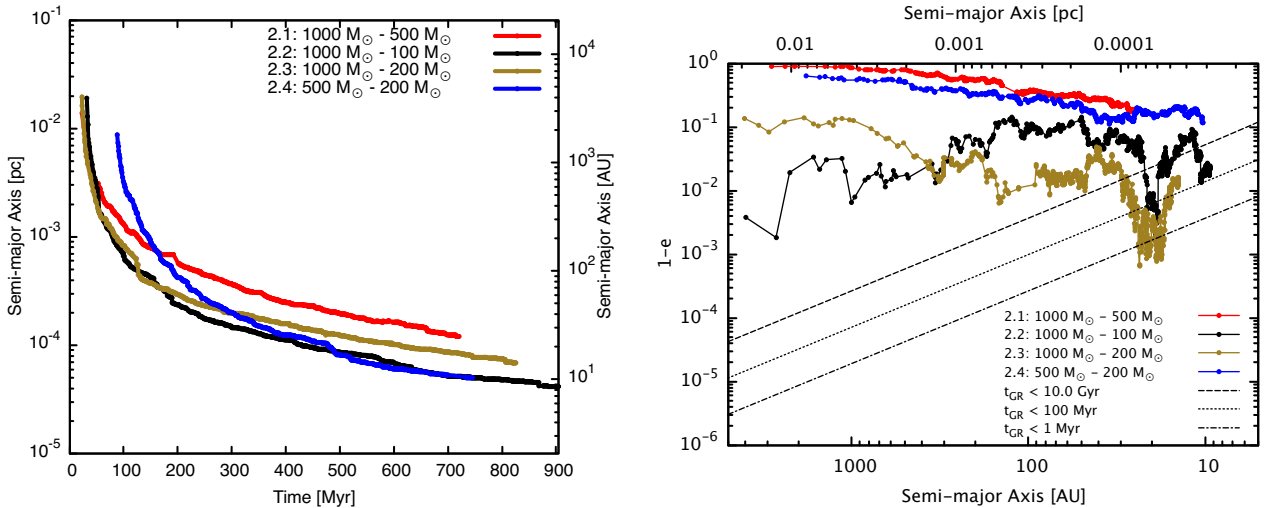


Figure 7. The left panel shows the evolution of the semi-major axis of the binary IMBH following its formation till the end of the run. The right panel shows the semi-major axis vs $1 - e$ for the binary in runs 2.i. Lines indicating the time needed for a $1000 M_\odot$ and a $100 M_\odot$ IMBH in a binary to merge via gravitational wave (GW) emission are also shown on the figure. The eccentricity in models 2.2 and 2.3 becomes quite large and the IMBH could merge through GW radiation within few to several hundred Myr respectively.

is shown in the left panel of Fig. 7. We find that in all these runs, the binary hardens with time and over the course of a few hundred Myr, the binary semi-major axis decreases from a few thousand AU to a few tens of AU. The binary hardens by scattering away stars in 3-body interactions. We find that in all the runs, this scattering away of stars by the binary also leads to systematic growth in its orbital eccentricity. The right panel in Fig. 7 shows evolution of the semi-major axis and the eccentricity of the binary in the 2.i runs. The evolution of the binary IMBH and the reason for the increase in eccentricity are discussed in Appendix A. The merger timescale due to GW emission strongly depends on the orbital eccentricity of a binary. As eccentricity approaches unity, the time needed for a binary to merge due to gravitational radiation emission decreases significantly as it depends on $(1 - e^2)^{\frac{7}{2}}$ (Peters 1964).

From the right panel in Fig. 7, it can be seen that the eccentricity

for the binary IMBH in runs 2.2 and 2.3 reaches very high values with $1 - e$ being less than 10^{-3} . The merger time due to GW emission for binaries with these eccentricities is less than a few hundred Myr. For runs 2.1 and 2.4, the eccentricity does not reach such high values, hence these binaries will take up to a few Gyr to merge. The main difference between runs 2.2, 2.3 and runs 2.1, 2.4 is the eccentricity at the formation of the binary (Nasim et al. 2020). Runs 2.2 and 2.3 form with moderately high eccentricity while the formation eccentricity is lower for runs 2.1 and 2.4. The initial eccentricity is driven by motion of the IMBH during the early phase of its inspiral and determines whether the binary can reach a high eccentricity state within a Gyr in order to effectively merge due to GW radiation. As discussed in Appendix A, the increase in binary orbital eccentricity due to binary-single scattering in these runs, which has also been shown in other studies, is most likely a

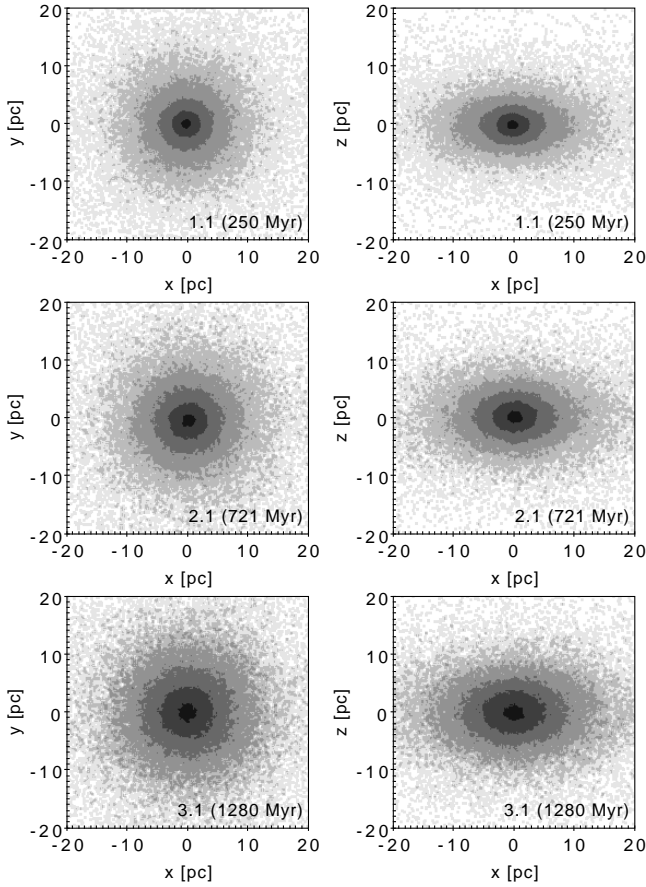


Figure 8. The three rows of figure show the density shaded $X - Y$ (left) and $X - Z$ (right) particle plots for runs 1.1 (top panel), 2.1 (middle panel) and 3.1 (lower panel) using the simulation snapshots at 250, 721 and 1280 Myr, respectively. The origin in these plots is the density centre of the merged cluster.

physical effect and does not rely on the assumptions or methods that are used. This includes methods and techniques such as scattering experiments, full N -body but low mass resolution and full N -body but low number of particles.

The initial setup of the merger between the clusters can impart a residual rotation on the final cluster. We find that the IMBH binary orbital plane is co-planar with respect to the merged cluster rotation plane for our runs. As discussed by Iwasawa et al. (2011), this can result in preferential ejection of stars on prograde orbits which can leave more stars on a retrograde orbit around the IMBH binary leading to transfer of angular momentum from the secondary to field stars resulting in an increase in eccentricity. This process has also been observed in the evolution of massive BH binary perturbed by a massive star cluster in a galactic centre (Arca Sedda et al. 2019b). Additionally, the setup of the merging clusters leads to flattening of the merged cluster in the Z direction. This ellipticity of the merged cluster can also further drive the hardening and eccentricity of the binary IMBH by rapidly refilling the loss cone (Khan et al. 2013, 2018, 2020). Fig. 8 shows the density shaded $X - Y$ and $X - Z$ plane plots of the merged cluster for runs containing 1, 2 and 3 IMBH at different snapshot times. From the plots it can be clearly seen that the cluster is flattened in the Z direction and the typical values of c/a axis ratio range between ~ 0.5 to 0.8 .

Table 4. Table showing the 3 simulated merging stellar cluster models that contain 3 IMBH. The description of columns is as that in Table 2. The runs have been labelled with the colours that are used for them in Figs. 11, 12 and 15.

Run	Time [Myr]	Total Mass [M_{\odot}]	IMBH ₁ [M_{\odot}]	IMBH ₂ [M_{\odot}]	IMBH ₃ [M_{\odot}]
3.1 •	1511	8.57×10^4	1000	500	200
3.2 •	832	8.57×10^4	500	1000	200
3.3 •	939	8.57×10^4	200	500	1000

5 SIMULATIONS CONTAINING THREE IMBHS (3.1 RUNS)

We simulated three runs in which each of the three stellar clusters in our original set-up (Section 2.1) initially had an IMBH at its centre. The masses of the IMBHs in the three merging stellar clusters were 1000, 500 and 200 M_{\odot} . The configuration of the IMBHs in the runs and the time for which they were run are given in Table 4.

In run 3.1, the central star cluster with 50 000 particles hosted a 1000 M_{\odot} IMBH, and the infalling clusters with 30 000 and 15 000 particles contained 500 and 200 M_{\odot} IMBHs respectively. In run 3.2, the initial position of the 1000 M_{\odot} IMBH was swapped with the 500 M_{\odot} IMBH. In run 3.3, the central star cluster with 50 000 particles contains the 200 M_{\odot} IMBH while the least massive stellar cluster with 15 000 particles hosts the 1000 M_{\odot} IMBH.

In all of the three runs, the 1000 and 500 M_{\odot} IMBHs segregate to the centre of the merged cluster to form a binary IMBH. We show the separation between the three IMBHs in Fig. 9.

Similar to the 2.i runs, the two IMBHs end up forming a binary on timescales of a few tens of Myr. In all these runs, the two most massive IMBHs end up in a binary at the centre of the merged cluster. In runs 3.1 and 3.3, the 200 M_{\odot} IMBH also sinks to the centre and reaches a separation of 10^{-2} pc from the binary IMBH. In both these runs, the 200 M_{\odot} IMBH is ejected from the merging clusters because of a strong encounter with the binary IMBH.

5.1 Run 3.1: Multiple strong binary-single IMBH scatterings

In run 3.1, we find that the third IMBH undergoes multiple strong encounters with the binary IMBH. The $X - Y$ position plot of the three IMBHs in run 3.1 is shown in Fig. 10. The binary IMBH forms with an eccentricity of 0.4. Initially, the evolution of the binary is similar to run 2.1 and we find that its eccentricity gradually increases as the semi-major axis decreases. However, frequent interactions with the third IMBH significantly modify the eccentricity evolution, as seen in Fig. 11. When the binary has a semi-major axis of around 200 AU, we see large changes in the eccentricity of the binary which are caused by interactions with the 200 M_{\odot} IMBH. The interaction which leads to the ejection of the 200 M_{\odot} IMBH takes place at about 580 Myr (see Fig. 9, leftmost panel). The binary remains intact and bound to the cluster, however, its trajectory within the cluster changes. The strong scattering that ejects the 200 M_{\odot} IMBH also causes a sharp decrease in eccentricity of the binary IMBH. The semi-major axis of the binary IMBH is 50 AU at this time. Subsequently, the eccentricity gradually increases again and evolves similarly to the 2.1 run. However, the hardening of the binary is slower compared to run 2.1 because frequent interactions between the three IMBH and surrounding stars after 100 Myr results in the ejection of a significant number of stars from the central part of the cluster. Also the recoil from the ejection of the third IMBH

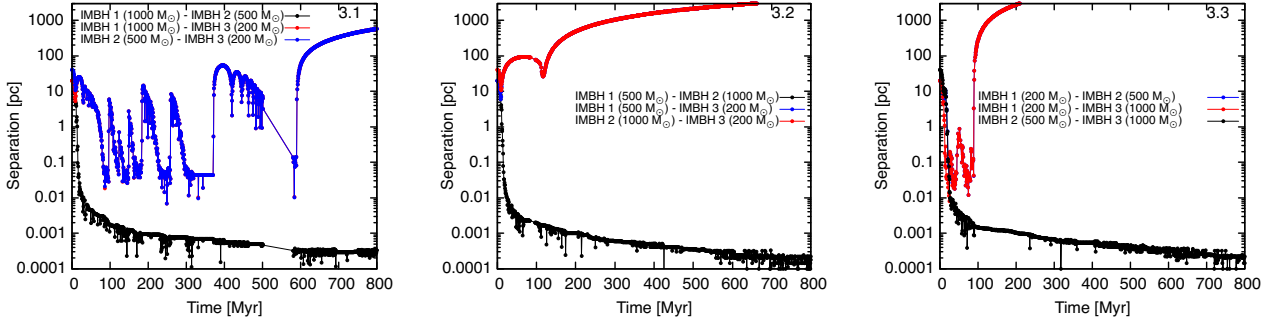


Figure 9. The three panels show the instantaneous separation between the three IMBHs in the 3.i runs. The non-smooth lines are due to the orbital eccentricity of the binary IMBH system. In all the 3.i runs, we form an IMBH binary consisting of the $1000 M_{\odot}$ and $500 M_{\odot}$ IMBH. For run 3.1, the precise data for the IMBHs between 500 to about 580 Myr was not available as they were part of a chain interaction in `NBODY6++GPU`.

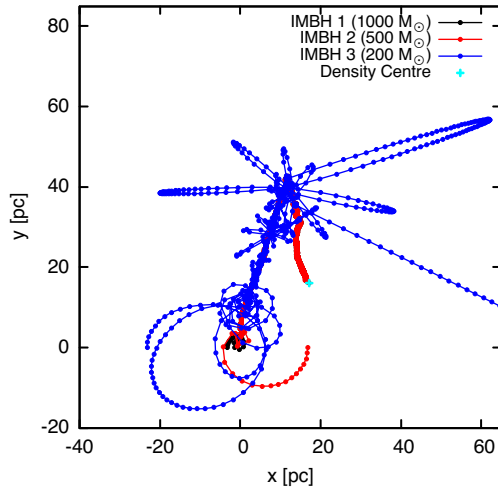


Figure 10. $X - Y$ position of the 3 IMBHs in run 3.1. The 1000 and $500 M_{\odot}$ IMBHs quickly form a close binary system within 25 Myr. The $200 M_{\odot}$ IMBH (shown in blue) slowly segregates to the cluster centre and a triple IMBH system forms. Subsequently the $200 M_{\odot}$ IMBH is scattered away from the inner binary IMBH repeatedly until it is finally ejected. The cyan cross indicates the $X - Y$ position of the centre of density at the last snapshot.

(see Section 6.2) puts the binary in a part of the cluster where the background stellar density and velocity dispersion is lower. The density of stars inside a box of 1 pc around the centre of mass of the binary IMBH at 582 Myr (shortly after the ejection) was $340 M_{\odot} \text{ pc}^{-3}$ for run 3.1, compared to $1126 M_{\odot} \text{ pc}^{-3}$ in run 2.1 (see left panel in Fig. 15). The slower hardening of the binary IMBH in run 3.1 after 580 Myr can also be seen in Fig. 12, which shows the evolution of the binding energy of the binary IMBHs in runs 2.i and 3.i. This slower hardening of the binary IMBH increases the time needed for it to merge due to GW radiation. Extrapolating the evolution of the gravitational wave merger time using the semi-major axis and eccentricity values for the IMBH binary from snapshots after 600 Myr, we estimate a merger time of around 6000 Myr. We find that after 1500 Myr of evolution, the IMBH binary is in close proximity ($\lesssim 0.2$ pc) to the cluster density centre.

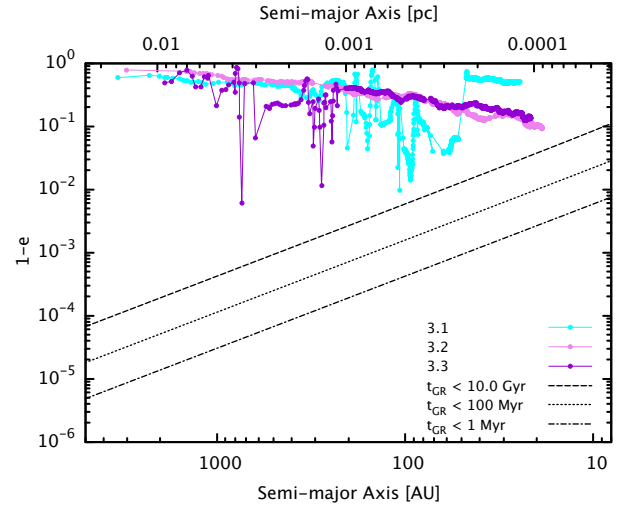


Figure 11. Semi-major axis vs $1 - \text{eccentricity}$ of the inner binary IMBH containing the $1000 M_{\odot}$ and $500 M_{\odot}$ IMBH in 3.i runs. The cyan line is for run 3.1, the violet line is for run 3.2 and the dark violet line is for run 3.3.

5.2 Run 3.2: Tidal stripping of third IMBH prevents triple formation

In run 3.2, as the merging clusters spiral in together, the $200 M_{\odot}$ IMBH is put on a wide orbit along with stars that are stripped away from its host cluster. The $200 M_{\odot}$ IMBH never comes close to the inner binary and hence does not affect its evolution. The semi-major axis and eccentricity evolve in a similar way to run 2.1, since the eccentricity of the binary at formation time is similarly low (0.2 for run 3.2 compared to 0.1 for run 2.1).

5.3 Run 3.3: Early ejection of the $200 M_{\odot}$ IMBH

In run 3.3, the $200 M_{\odot}$ IMBH is ejected following an interaction with the binary IMBH at around 90 Myr. At this time, the semi-major axis of the binary is about 200 AU (~ 0.001 pc; see Fig. 9). Prior to the ejection, the eccentricity of the binary fluctuates due to dynamical interactions with the $200 M_{\odot}$ IMBH. Following this interaction, the eccentricity and semi-major axis of the binary evolve in a similar way to run 2.1. Unlike run 3.1, the interaction that ejects the third IMBH occurs earlier in the evolution of the system when the binary semi-major axis is large. This leads to a lower recoil

velocity for the binary and it remains in the centre of the merging cluster where the background stellar density is high.

5.4 Summary of simulations containing three IMBHs

In summary, the 3.i runs show diverse outcomes. In run 3.1, the third IMBH stays within the merged cluster for a few hundred Myr before it is ejected in a binary-single scattering. In run 3.2, the lowest mass IMBH ends up on a wide orbit and never dynamically interacts with binary IMBH. In run 3.3, the binary IMBH and the third IMBH have a strong encounter that leads to the ejection of third IMBH within a 100 Myr from the start of the simulation; again, it does not affect the subsequent evolution of the binary.

Similarity in the hardening of the binary IMBH in runs 2.1, 3.2 and 3.3 can be seen in Fig. 12. The binding energy of the IMBH binaries ($1000 M_{\odot} - 500 M_{\odot}$) in all three runs increases at a nearly constant rate of $1.1 \times 10^4 M_{\odot} \text{ km}^2 \text{ s}^{-2} \text{ Myr}^{-1}$. In comparison, for run 3.1, the binary hardens at a slower average rate of $7.6 \times 10^3 M_{\odot} \text{ km}^2 \text{ s}^{-2} \text{ Myr}^{-1}$. As discussed in Section 5.1, the binary IMBH strongly interacts with the $200 M_{\odot}$ IMBH during the first 580 Myr of its evolution this results in the ejection of stars from the inner regions of the merged cluster. Eventually, the $200 M_{\odot}$ IMBH is ejected and the binary hardening rate is slowed down due to a lower background stellar density.

We have also calculated the time-dependent binary hardening rate (Quinlan 1996):

$$s \equiv \frac{d}{dt} \left(\frac{1}{a} \right) \quad (1)$$

by calculating the gradient of the $a^{-1}(t)$ evolution over fixed intervals from the time of the binary formation to the end of the simulations (similar to Gualandris & Merritt (2012); Arca-Sedda & Gualandris (2018)). As previously discussed, the hardening of the IMBH binary is higher for the lower mass ratio binaries in runs 2.2 and 2.4. The density of stars around the IMBH binary is also higher in these runs. For runs 2.1, 3.2 and 3.3, the hardening rate is roughly constant. For run 3.1, the presence of the third IMBH in the cluster slows down the hardening rate of the IMBH binary. However, as the model evolves beyond 800 Myr, the hardening rate of the IMBH binary is beginning to increase as it settles back into the cluster centre.

5.5 Cluster density evolution and stellar properties

Using the runs described in previous sections, we have also checked how the cluster density structure evolves and what influence the presence of an IMBH or IMBH binary has on the cluster density profile. It was shown in Fig. 5 that the density profile of the run with no IMBH and the runs with 1 IMBH were similar after a few hundred Myr of cluster evolution. In the two panels of Fig. 13, we show the evolution of the cluster density profile for runs 0.1 (top panel) and 1.2 (bottom panel) using simulation snapshots. For each snapshot, the position of the density-weighted centre was found using the procedure described in de Vita et al. (2018). In both these runs, we find that the central density of the cluster increases by a factor of 2-3 at around 360 Myr of evolution. The central density of a merged cluster is expected to increase with time as it dynamically evolves (Mastrobuono-Battisti et al. 2019). The presence of an IMBH also leads to a slightly steeper inner density profile. A similar evolution for the density profile is also observed for runs 1.1 and 1.3.

Table 5. This table provides the estimated bound cluster mass and half-mass radius of the clusters close to end of the simulation.

Run	Time [Myr]	Cluster Mass [$\times 10^4 M_{\odot}$]	Half-Mass Radius [pc]
0.1	375	7.7	2.30
1.1	250	7.5	2.28
1.2	357	7.5	2.30
1.3	551	7.5	2.32
2.1	716	7.2	2.76
2.2	914	7.5	2.70
2.3	825	7.5	2.61
2.4	745	7.4	2.57
3.1	1511	6.7	3.48
3.2	832	7.1	2.68
3.3	939	7.3	2.91

In the case of the runs 2.i and 3.i, the formation of the IMBH binary leads to a slight decrease in the central density with time as surrounding stars are scattered away due to interactions with the IMBH binary as it gradually hardens (see Appendix A). The evolution and shape of the density profile is similar between runs 2.1, 3.2 and 3.3. The inner density profile (within 2 pc) for these runs is also steeper compared to runs 2.2 and 2.4 owing to the larger mass of the IMBH binary. Fig. 14 shows the evolution of the density profile for runs 2.1, 2.2, 3.1 and 3.2. The density profile for run 3.1 decreases steeply within the inner 2 pc after 400 Myr due to the scattering of the third IMBH (see Section 5.1 and Fig. 9).

Using the profiles shown in Fig. 13 and Fig. 14. We fit the density profile to a power-law function given by $\rho(r) \propto r^{-\gamma}$. We find that γ ranges between 1.2 and 1.6 and tends to increase with the evolution time of the cluster. These values are consistent with observationally inferred density profiles of NSCs (Neumayer et al. 2020; Pechetti et al. 2020).

The left panel of Fig. 15 shows the stellar density around the IMBH calculated within a radius of 0.25 pc. We find that the highest stellar density around the IMBH binary is for run 2.1 which also accounts for why its hardening is faster compared to the other runs (see Appendix A). We also find that the average mass surrounding the IMBH binary in all the 2.i and 3.i runs is gradually increasing with time. This can be seen in the right panel of Fig. 15. As the merged cluster evolves, more massive stars segregate closer to the centre (Panamarev et al. 2019) and the IMBH binary. Table 5, shows the approximate bound cluster mass (within ~ 15 pc) and half-mass radius for the runs towards the end of the simulations. Stellar ejections also play a role in the cluster evolution and the evolution of the binary IMBH (Iwasawa et al. 2011; Wang et al. 2014). The bound cluster mass about 80 - 90 per cent of the initial cluster mass and is smaller for more evolved models and those with a more massive IMBH binary.

6 THE FATES OF IMBHs IN MERGING STELLAR CLUSTERS

In this section, we discuss the fates of IMBHs that are delivered to the centre of a galaxy. In the runs presented in Sections 4 and 5 we show that multiple IMBHs could potentially be delivered to the NSC. Whilst we expect that a single IMBH would always be retained in the NSC following delivery, two additional mechanisms can act if multiple IMBHs are present.

In both the 2.i and 3.i runs, we find that a binary IMBH forms

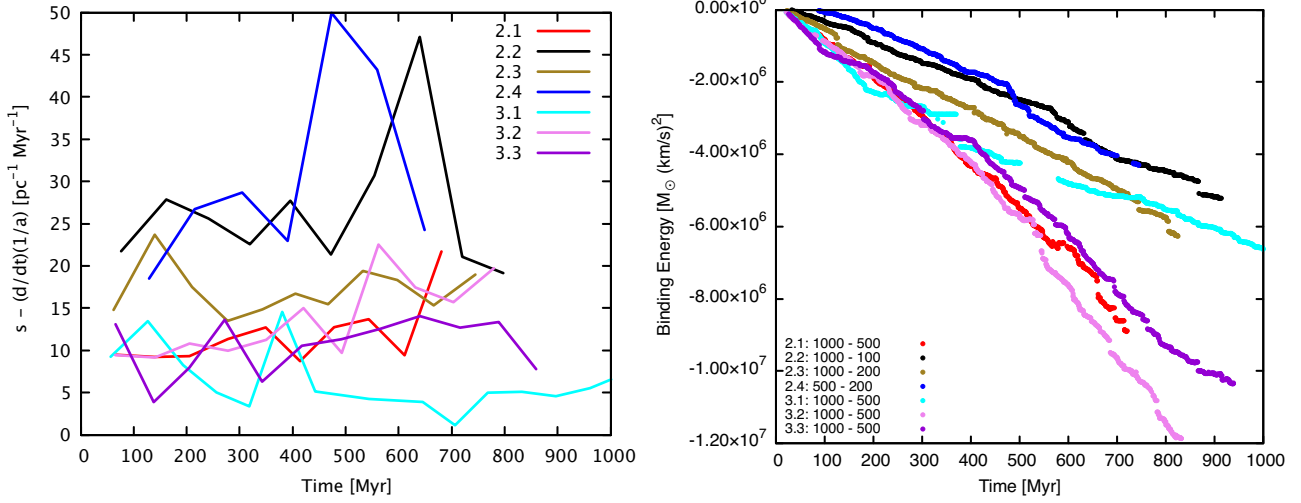


Figure 12. The left panel shows the evolution of the time dependent hardening rate (Equation 1) of the binary of the binary IMBH in the 2.i and 3.i runs. The right panel shows the evolution of the binding energy of the binary IMBH.

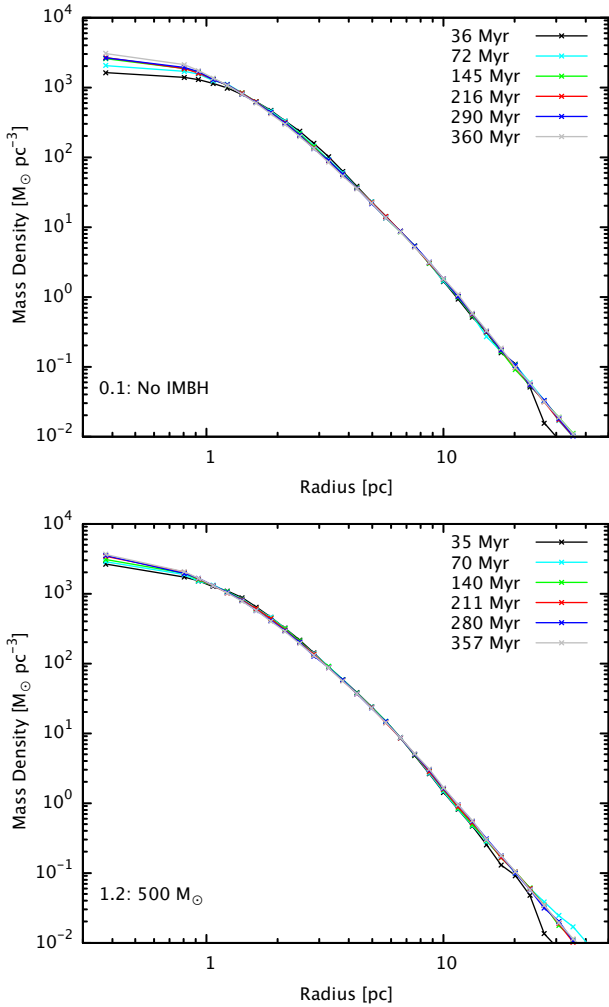


Figure 13. The two panels show the evolution of the radial density profile of the merged cluster for runs 0.1 (top) and 1.2 (bottom).

and gradually hardens and becomes more eccentric. These binaries can efficiently merge through GW radiation on timescales of a few hundred Myr to a few Gyr. However, the merger will lead to a recoil kick from asymmetric emission of gravitational waves (Fitchett 1983; Merritt et al. 2004). This kick could remove the merger product from the NSC, leaving behind no seed black hole to grow into an SMBH. In Section 6.1, we discuss gravitational recoil kicks and the role they play in removing IMBH from the NSC.

Binary-single scatterings involving IMBHs could lead to the ejection of the single IMBH from the cluster, and possibly also the ejection of the binary. In Section 6.2, we discuss binary-single encounters involving three IMBHs, the possible outcomes, and their dependence on the properties of the interacting IMBHs.

If an IMBH is retained in the NSC then it can seed the formation of an SMBH. In Section 6.3, we discuss the main processes by which an IMBH could grow in an NSC in order to become an SMBH. In Section 6.4, we discuss the caveats and limitations of the runs that we presented and how they may impact the results.

6.1 GW recoil kicks and IMBH retention

In Sections 4 and 5, we found that in all of our runs that contained two or more IMBHs, a binary IMBH forms within a few tens of Myr, which then gradually hardens and becomes more eccentric by scattering away stars (Appendix A). The merger time for a binary inspiralling due to GW radiation (Peters 1964) is given by:

$$\tau_{\text{gr}} \approx 10^{10} \text{ yr} \left(\frac{a_{\text{bin}}}{3.3 R_{\odot}} \right)^4 \frac{1}{(m_1 + m_2) m_1 m_2} \cdot (1 - e^2)^{7/2} \quad (2)$$

where a_{bin} is the semi-major axis of the binary, e is the eccentricity, and the masses of the two black holes are m_1 and m_2 in solar mass.

As the eccentricity of the binary increases, the GW inspiral time given by Equation 2 decreases. We find that for runs 2.2 and 2.3, the binaries will merge within 500 Myr from the start of the simulation. Extrapolating, the evolution of the semi-major axis and eccentricity for the binary in runs 2.1, 3.2 and 3.3, we estimate the merger time to be around 1500 Myr. For run 2.4, we find a merger time of around 1000 Myr. The longest estimated merger time for

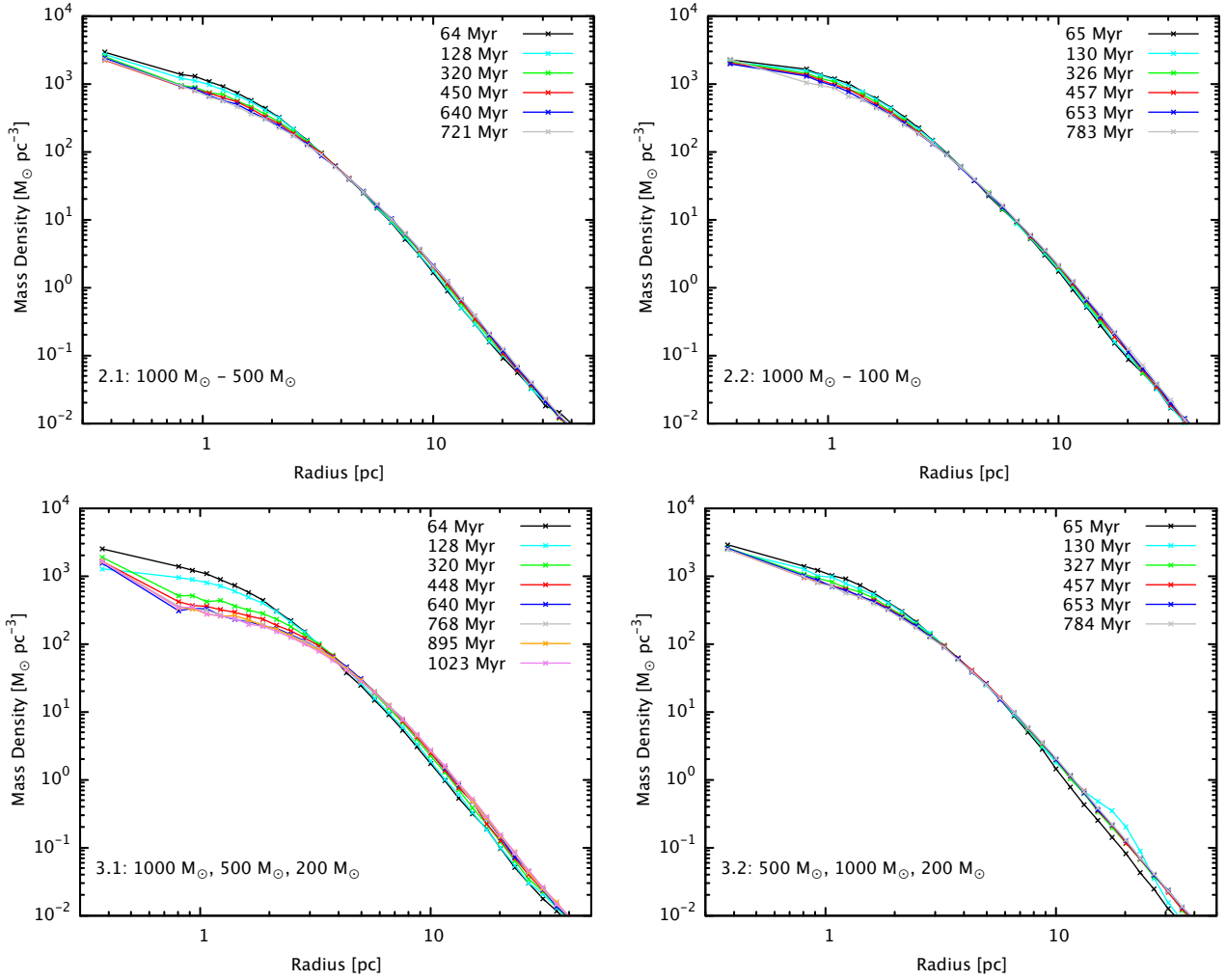


Figure 14. The top two panels show the evolution of the density profile of runs 2.1 (left) and 2.2 (right). The lower two panels show the evolution of the density profile for runs 3.1 and 3.2.

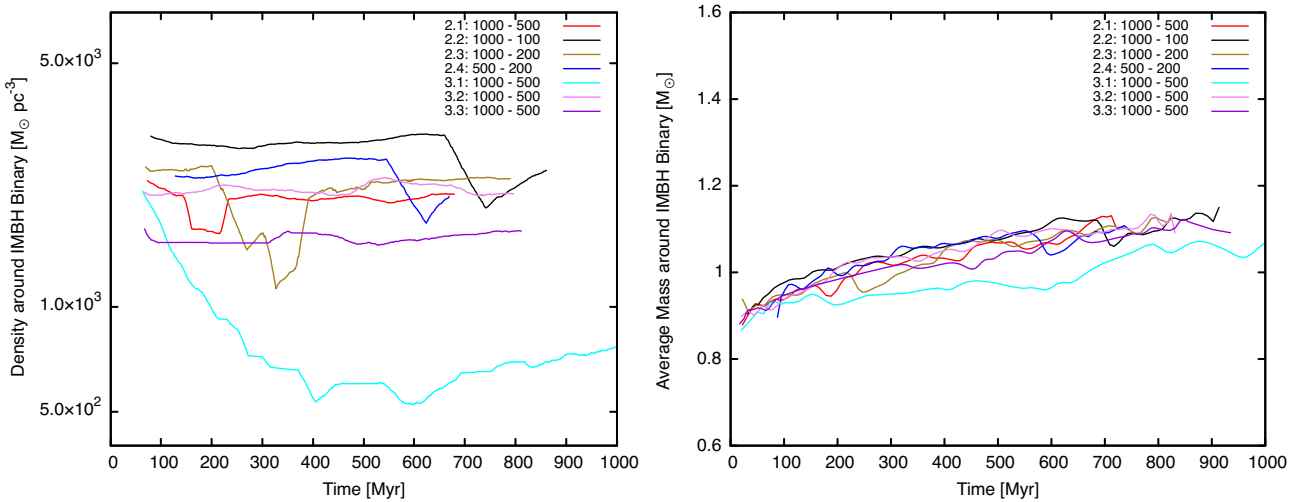


Figure 15. The left panel show the evolution of the density surrounding the IMBH binary in runs 2.i and 3.i. The right panel shows the average mass of the stars in the vicinity of the IMBH binary. The density and average stellar mass were calculated inside a box with length 0.5 pc centered on the centre of mass of the IMBH binary.

Table 6. This table provides the estimated merger time for the IMBH binaries in runs 2.i and 3.i.

Run	IMBH Binary Mass [M_{\odot}]	Estimated GW Inspiral Time [Myr]
2.1	1000 M_{\odot} - 500 M_{\odot}	1500
2.2	1000 M_{\odot} - 100 M_{\odot}	500
2.3	1000 M_{\odot} - 200 M_{\odot}	500
2.4	500 M_{\odot} - 200 M_{\odot}	1000
3.1	1000 M_{\odot} - 500 M_{\odot}	6000
3.2	1000 M_{\odot} - 500 M_{\odot}	1500
3.3	1000 M_{\odot} - 100 M_{\odot}	1500

the IMBH binary is 6000 Myr for run 3.1. Table 6 summarizes the estimated merger times for the different IMBH binaries in our runs. The extrapolation was done by fitting the evolution of the gravitational wave merger time calculated from the semi-major axis and eccentricity evolution from snapshots following the formation of the IMBH binary. As discussed in Section 5.1, following a strong interaction with a single IMBH, the binary eccentricity decreases and the subsequent recoil from the interaction places the binary in the part of the cluster where the stellar background density is low and thus the hardening rate for the binary decreases leading to a longer merger time. However, given that the timescale for hardening and eccentricity pumping depends on the density and velocity dispersion of stars around the binary IMBH, in a denser cluster the time needed for the binary to merge due to GW radiation may be a lot shorter (Rasskazov et al. 2019). However, it may not be so straightforward to extrapolate our results to denser systems. This is discussed in more detail at the end of Section 6.4.

The GWs emitted by binary BHs as they inspiral are anisotropic. As the final inspiral occurs in less than one orbital period of the binary, the GWs carry away linear momentum. In order to compensate for this, the merged BH acquires a GW recoil kick (Fitchett 1983; Wiseman 1992). The magnitude of this recoil kick depends strongly on the mass ratio of the merging BHs and their relative spin magnitudes and orientations (Baker et al. 2007, 2008; González et al. 2007; Campanelli et al. 2007; Lousto & Zlochower 2008; Lousto et al. 2012). For a perfectly symmetric binary system, comprising equal mass non-spinning BHs, the recoil kick will be zero; however, large spin values with asymmetric orientations can lead to recoil kicks that can be of order of a few thousand km s^{-1} (Holley-Bockelmann et al. 2008; Lousto et al. 2012; Blecha et al. 2016; Fragione et al. 2018a). Such kicks can eject the merged BH from its host NSC (Holley-Bockelmann et al. 2008; Campanelli et al. 2007; Morawski et al. 2018; Gerosa & Berti 2019; Dunn et al. 2020). Mergers with more extreme mass ratios result in lower recoil kicks, and the merged remnant is more likely to be retained in dense environments with relatively large escape velocities (Morawski et al. 2018; Antonini et al. 2019; Rodríguez et al. 2019; Fragione & Silk 2020).

In order to estimate the dependence of recoil kick velocities on the mass ratio of merging IMBH, we sampled a set of 10^5 merging binary BHs with a uniform mass ratio distribution. A spin value was assigned to each BH by combining the ‘hot’ and ‘cold’ spin distributions provided in Fig. 7 of Lousto et al. (2012). These spin distributions have a peak value of about 0.7 and take into account the accretion-driven growth of the BHs. Given that the binary IMBH in our clusters form dynamically, we assume an isotropic distribution of spin orientations. For each binary we then estimate the recoil kicks based on fits to results from numerical relativity simulations provided by Baker et al. (2008); van Meter et al. (2010) and average

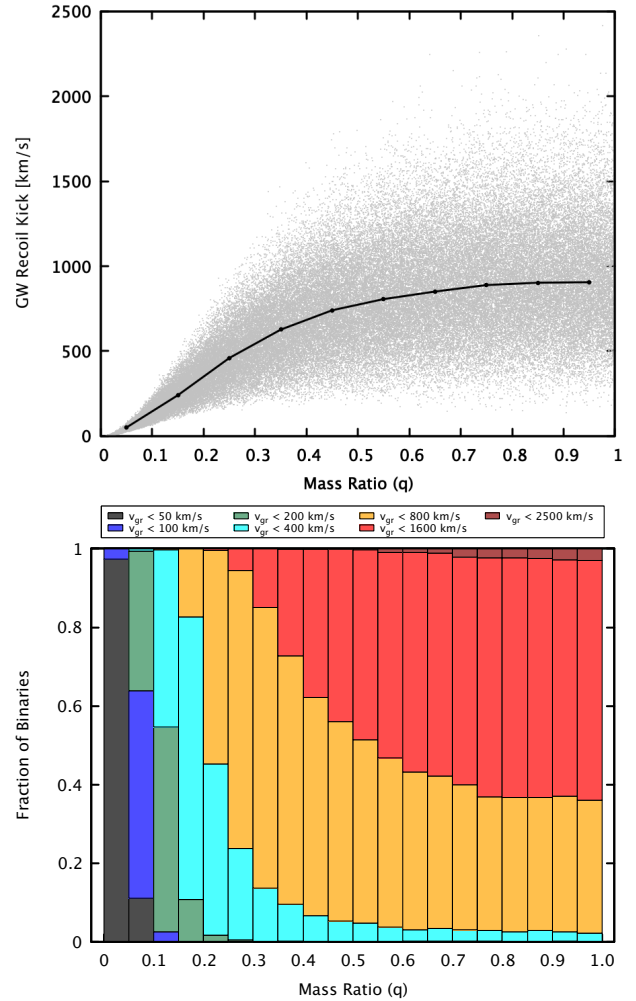


Figure 16. The top panel shows the gravitational wave recoil kick (v_{gr}) as a function of the mass ratio (q) for 10^5 merging BHs with a uniform mass ratio distribution. The black line shows the median value of recoil kicks, as a function of mass ratio. The lower panel histogram shows the fraction of binaries with recoil kick velocities lower than 50, 100, 200, 400, 800, and 2500 km s^{-1} as a function of mass ratio.

over five different spin orientations for each binary. The GW recoil velocity as a function of mass ratio is shown in Fig. 16. We find that for the majority of the binaries with mass ratio $q \lesssim 0.15$, the median recoil velocities would be of the order $\lesssim 200 \text{ km s}^{-1}$. In that case, the merged IMBH could be retained in NSCs where escape speeds are of the order of a few hundreds of km s^{-1} (Antonini et al. 2019; Gerosa & Berti 2019). For higher mass ratios of the merging BHs, GW recoil velocities can be much higher due to spin asymmetry leading to a significant contribution in the recoil kick velocity vector which is perpendicular to the orbital plane (Baker et al. 2008; van Meter et al. 2010; Lousto et al. 2012).

For our runs where the mass ratio of the binary IMBH is less than about 0.15 (as in runs 2.2 and 2.3), the likelihood for the merged remnant to receive a low kick and be retained in a dense NSC will be higher. These are also the runs in which GW radiation merger times for the binaries are the shortest. For higher mass ratios, the likelihood for the merged BH to be ejected out of the NSC will increase. This process can result in the ejection of the IMBH from an NSC. Therefore, GW recoil kicks have an important consequence

on whether or not an NSC can retain an IMBH that can go on to seed an SMBH (Merritt et al. 2004; Volonteri 2007).

Similarly, GW recoil kicks are also important from the point of view of forming IMBHs in dense stellar clusters. If the initial seed BH forms from the collapse of a massive star created through runaway collisions and is of the order of a few hundred solar masses then the likelihood of retaining the seed following mergers with lower mass stellar BHs will be higher (Baker et al. 2008; van Meter et al. 2010; Morawski et al. 2018). However, depending on initial spin distributions of BHs, slow growth of a low mass seed BH through mergers with other stellar-mass BHs of similar mass is likely to eject the seed from the cluster which will inhibit IMBH formation (Rodríguez et al. 2019; Gerosa & Berti 2019).

6.2 2+1 Scattering

Here we consider the effects of a binary-single encounter between three IMBHs and the consequences these interactions can have on the retention of IMBH in the merged cluster. Such encounters occur in our run 3.1 and could potentially result in the escape of one or multiple IMBHs. Here we estimate the recoil velocities that can come out of such interactions and under which circumstances could all three IMBHs be potentially removed from the NSC.

If we assume that we have a hard binary IMBH that has a binding energy which is much larger than the kinetic energy of the single IMBH that it encounters, then by conserving energy and momentum in the rest-mass frame of the encounter, we can estimate the resulting recoil speed of the binary to be

$$V_{\text{bin}} = \sqrt{\alpha \frac{m_1 m_2 m_3}{(m_1 + m_2)(m_1 + m_2 + m_3)}} \cdot \frac{1}{a} \cdot 30 \text{ km s}^{-1} \quad (3)$$

where m_1 and m_2 are the masses of the binary components and m_3 is the mass of the single. The masses are in units of M_\odot and a is the semi-major axis of the binary in units of AU. α is the fractional change in the binding energy of the binary following the interaction, i.e. $\Delta E_b / E_b$. For a hard binary, α is proportional to the ratio between the mass of the single and the mass of the binary.

For the 3.i runs, the component masses of the binary IMBH are $m_1 = 1000 M_\odot$, and $m_2 = 500 M_\odot$, and the mass of the single IMBH is, $m_3 = 200 M_\odot$. Taking $\alpha = 0.1$ (Hills 1983), the binary recoil velocity can be expressed in terms of the semi-major axis of the binary as

$$V_{\text{bin}} = 59.41 \text{ km s}^{-1} \sqrt{\frac{1}{a}} \quad (4)$$

In the context of runs 3.i, for the inner binary IMBH to receive a significant recoil kick ($> 50 \text{ km s}^{-1}$) in an interaction with the $200 M_\odot$ IMBH, its semi-major axis should be at most 1.4 AU. For a higher α value of 0.3, this semi-major axis would be 4.2 AU. However, the $200 M_\odot$ IMBH is more likely to be ejected out before the semi-major axis hardens to reach such a small separation and this is shown in all the 3.i runs. In runs 3.1 and 3.3, we find that the single IMBH is ejected from the cluster following a strong encounter with the binary IMBH at a time when the binary semi-major axis values are 50 AU and 200 AU.

If an additional IMBH is delivered to the NSC while the binary IMBH has hardened to about an AU, then a binary-single scattering could result in significant recoil velocity for the binary IMBH and this can potentially eject all three IMBHs from a NSC (Gültekin et al. 2006) with escape velocities of the order of several tens of

km s^{-1} . However, according to Equation 2, the GW radiation merger time for a binary IMBH with component masses of $1000 M_\odot$ and $500 M_\odot$, with a separation of 1 AU and an eccentricity of 0.9, is around 1 Myr. This merger timescale for the binary IMBH is much shorter than the expected injection frequency of an additional IMBH into the NSC which may occur on timescales of about a 100 Myr to up to 1 Gyr. Therefore, the likelihood of a single IMBH to encounter the binary IMBH while it is hard enough to get a significant recoil velocity is small. The most likely outcome of an interaction between the binary IMBH and a single IMBH is either ejection of the single IMBH or its exchange with one of the binary components.

Interactions between a binary IMBH and another IMBH can influence the eccentricity evolution of the binary described in Appendix A. In run 3.1, we found that the merger time for the binary IMBH becomes longer following an interaction with the third IMBH which leads to ejection of the latter. This interaction decreases the eccentricity of the binary which increases its merger time. In runs 3.i, all three IMBH were there from the very beginning. However, if the third IMBH is delivered with a merging cluster after a few hundred Myr of the formation of the binary IMBH then it is likely that the binary IMBH has already hardened and become sufficiently eccentric that it would merge before it encounters the third IMBH (see Section 6.2). Other works have investigated triple interactions between IMBH/SMBH in nuclei of galaxies (Hoffman & Loeb 2007; Arca-Sedda & Capuzzo-Dolcetta 2019) and found that such encounters can lead to erratic changes in the orbital eccentricity of the binary which could drive their prompt merger. Additionally, it has also been found that such interactions could lead to the ejection of BHs from the nuclei to the halo of the galaxy.

6.3 Growing seeds to super-massive black holes

We argue that if an NSC forms through mergers of stellar clusters then it is possible that some of these merging clusters may bring along IMBHs. These IMBHs can potentially grow in the galactic nuclei in order to become SMBHs. However, if the merging clusters do not bring along an IMBH then the nuclei will not contain a seed BH that can grow on to become an SMBH.

In run 0.1, we showed that the merger of three stellar clusters without any IMBH can lead to the formation of a merged cluster with a dense core. Relatively low mass galaxies that have NSC masses of the order of few $10^6 M_\odot$ (like M33) may have formed their NSC through the merger of just a few stellar clusters. It is probable that none of these merging clusters contained an IMBH and therefore no IMBH is delivered to the galactic nuclei in these galaxies. If one IMBH is delivered to a galactic nucleus (runs 1.i) then the IMBH can stay in the nucleus where it can grow by either accreting gas or tidally disrupting stars (Devecchi & Volonteri 2009; Davies et al. 2011; Stone et al. 2017; Fragione et al. 2018b; Natarajan 2020). The stellar clusters that merge to form an NSC may also contain gas that could be delivered to the galactic nuclei (Davies et al. 2011; Guillard et al. 2016). Additionally, infall of gas into an NSC can also occur during galaxy mergers (Mayer et al. 2010). Gas in the NSC can be efficiently accreted by the IMBH (Leigh et al. 2013; Inayoshi et al. 2016; Sakurai et al. 2017; Natarajan 2020) and can result in the growth of the NSC by triggering in-situ star formation (Neumayer et al. 2020). Such inflow of gas will also effectively contract the NSC (Davies et al. 2011), leading to higher central densities which would increase the rate of tidal disruption events.

Miller & Davies (2012) argued that in dense NSCs with velocity dispersions larger than 40 km s^{-1} , binaries will be unable to support against core collapse which will lead to the runaway growth

of BHs. Stone et al. (2017) showed that in such NSCs, stellar BHs can become more massive by growing through tidal capture and disruption of stars. These tidal disruptions events can effectively grow the mass of a BH mass from $10^{2-3} M_{\odot}$ to up to $10^5 M_{\odot}$ (Stone et al. 2017; Alexander & Bar-Or 2017; Sakurai et al. 2019; Alister Seguel et al. 2020). IMBH can also grow by tidally disrupting white dwarfs (Rosswog et al. 2009; MacLeod et al. 2016). In addition to gas accretion, these dynamical processes can lead to the growth of the seed SMBH to larger masses. Furthermore, if the NSC grows through additional mergers of stellar clusters or gas accretion this could then replenish the environment around the seed SMBH.

In our simulated runs with two or more IMBH, we find that a binary IMBH forms. The binary IMBH scatters away stars and becomes more eccentric with time (Appendix A). Due to this increased eccentricity, the binary can efficiently merge due to GW radiation. As discussed in Section 6.1, after such a merger, the merged IMBH can receive a significant recoil kick which can be up to a few thousand km s^{-1} and can eject the IMBH from the NSC. This can remove the seed SMBH from the merged galaxy. However, if the recoil kick velocity is less than the escape speed of the NSC then the merged IMBH can be retained. The recoil velocity is lower for merging BHs with more extreme mass ratios. Therefore, if the initial seed IMBH in an NSC can grow its mass through gas accretion and/or tidal disruption of stars then the likelihood of retaining the seed following subsequent mergers with lower mass IMBHs will be higher (Blecha et al. 2011). These mergers can also contribute to the growth of the seed SMBH in the NSC.

6.4 Caveats and limitations

In this subsection, we discuss the main limitations of our simulated runs and discuss how those limitations may influence the results presented in this paper.

For our merging stellar clusters, we use a limited mass function with stars not more massive than $2 M_{\odot}$. The main sequence turn-off age for $2 M_{\odot}$ stars is about 800 Myr for a metallicity of $Z = 0.001$. Up to few hundred Myr of cluster evolution may be needed to form an IMBH of around a $1000 M_{\odot}$ in the individual cluster models that were merged together and by this time stars with a mass larger than $3 M_{\odot}$ would have already evolved. Therefore, the average mass of stars would still be significantly smaller than the mass of the IMBHs in the cluster. It can be expected that many of the stellar-mass BHs that form in these clusters are ejected due to natal kicks or have merged with the IMBH (Lützgendorf et al. 2013b; Leigh et al. 2014; Giersz et al. 2015; Hong et al. 2020). However, it is possible that there may still be few tens to hundreds of stellar mass BHs retained in the cluster at the time when the clusters fall in and merge. The inclusion of stellar-mass BHs in the initially merging clusters could potentially influence the eccentricity evolution of the binary IMBH discussed in Appendix A through strong dynamical interactions with the binary IMBH. Additionally, the presence of an IMBH in a stellar cluster can also result in mergers of stellar BHs binaries through Lidov-Kozai oscillations (Haster et al. 2016; Fragione & Bromberg 2019; Martinez et al. 2020; Samsing 2018). We will investigate the influence of including stellar-mass BHs within our merging stellar cluster models in a future study.

For simplicity, we did not consider any primordial binaries in our merging cluster set-up. Stars in primordial binaries may not have a significant influence on the segregation and formation of a binary IMBH. However, stellar-mass BHs in binaries could strongly interact with IMBHs as they segregate to the cluster centre. The MOCCA models described in Section 3.1 that do form an IMBH

contain both primordial binaries and BHs. These BHs either merge with the IMBH or are ejected out of the cluster through dynamical interactions (Giersz et al. 2015).

Additionally, our merged stellar clusters are not of the same size or density as NSCs observed in galaxies like M33 or the Milky Way. The estimated upper limit for mass of the NSC in M33 is $2 \times 10^6 M_{\odot}$ (Kormendy & McClure 1993; Graham & Spitler 2009) and Gordon et al. (1999) found the mass of the M33 NSC to be about $7 \times 10^5 M_{\odot}$. To keep a manageable number of stars in our simulated runs, we had scaled down the initial mass of the merging clusters and their initial densities were of the order of $10^3 M_{\odot} \text{pc}^{-3}$. It can be expected that the clusters merging with the galactic centre will be more massive and dense (Hartmann et al. 2011; Antonini et al. 2012). Having more dense and massive clusters with larger escape velocities will increase the likelihood of those clusters forming and retaining an IMBH (Antonini et al. 2019). Higher stellar density and velocity dispersion may also increase the hardening rate (Rasskazov et al. 2019), hence decreasing the time needed for the binary IMBH to merge due to GW emission. Additionally, it would also lead to faster growth of the seed SMBH in the NSC (Stone et al. 2017) as discussed in Section 6.3. However, there are several effects that may affect the binary evolution in denser systems. Firstly, dynamical friction would be less efficient and the IMBH in-spiral phase may last longer. Secondly, the hard binary separation would be smaller and therefore the binary separation would need to shrink sufficiently before stellar hardening becomes dominant. Thirdly, the influence radius of the IMBH binary would be much smaller and this would influence the orbit of stars surrounding the IMBH binary. This can imply less efficient refilling of the binary loss-cone and may lead to less efficient hardening of the IMBH binary. Lastly, the models presented here do not account for the tidal field exerted from the inner galaxy ($\lesssim 100 \text{ pc}$) onto the infalling clusters, which can significantly strip out the outer layer of the smaller clusters and potentially reduce the capability of the cluster nucleus to reach the innermost regions of the galactic centre.

7 CONCLUSIONS

In this paper, we have considered the idea that an NSC forms first and that the SMBH grows later. In this scenario, the formation of an NSC occurs through mergers of stellar clusters in a galactic nuclei. Some of these clusters may have formed IMBHs in them through dynamical processes described in Section 3.1. As the clusters merge, those IMBH(s) are delivered to the galactic nuclei where they can potentially grow and become seed SMBHs (Ebisuzaki et al. 2001).

In order to investigate the viability of this scenario, we simulated the final stages of an idealized merger of three stellar clusters to form a merged cluster using N -body simulations. We consider a range of cases where various combinations of the three merging clusters can contain IMBHs. In our simulated runs, we have a hierarchy of masses in the merging stellar clusters: the mass of the IMBH ($100\text{--}1000 M_{\odot}$) is smaller than the mass of the three merging stellar clusters (up to $8 \times 10^4 M_{\odot}$) and the masses of stars (0.5 to $2.0 M_{\odot}$) in our cluster are smaller than the IMBH mass ($M_{\star} \ll M_{\text{imbh}} \ll M_{\text{cluster}}$). Additionally, there is no pre-existing SMBH in our simulations.

Since $M_{\text{imbh}} \ll M_{\text{cluster}}$, the properties of the merged cluster are not significantly influenced by the presence of an IMBH. For runs that do contain an IMBH, the timescale for segregation of the IMBHs to the merged cluster centre is of the order of a few tens of Myr. Additionally, given that $M_{\text{imbh}} \gg M_{\star}$, this leads to efficient

segregation of the IMBH(s) to the centre of the merged cluster due to dynamical friction.

For our runs with two or more IMBHs, we find that the IMBHs sink to the centre of the merged cluster (within 30 - 80 Myr) resulting in the formation of a binary IMBH. This binary hardens by scattering stars and becomes significantly eccentric in the process. Due to this increase in eccentricity, the time needed for the binary to merge due to GW emission decreases significantly. We found that the time needed for the merger of the IMBH binary ranges from several hundred Myr to a few Gyr. As discussed in Section 6.1, the retention of the merged IMBH will depend on the magnitude of the GW recoil kick. These kicks depend on the mass ratio of the merging BHs, and their spin magnitudes and orientations. We argue that the merged BH can be retained in typical NSCs provided that the mass ratio of the merging IMBH is low ($q \lesssim 0.15$), otherwise gravitational recoil kicks can be larger than a few hundred km s^{-1} and can remove the merged BH from the NSC. Additionally, if the binary IMBH dynamically interacts with a third IMBH within the NSC then this can lead to the ejection of the third IMBH or, in an unlikely case, the ejection of all three IMBHs. Given these different outcomes, NSCs constructed through merging clusters will either contain no seed BHs or they will retain a single seed IMBH that can further grow to become an SMBH.

This scenario would naturally explain the absence of SMBHs in galaxies like M33, where there was either no seed SMBH in the NSC to begin with or the product of the merger of two IMBHs was ejected due to GW recoil kicks. In massive galaxies with more massive NSCs, a higher number of clusters could have merged with the NSC which would increase the likelihood of delivering an IMBH which could then grow on to become an SMBH. In a companion paper, we model the build up of NSCs for a population of galaxies by merging stellar clusters. In these NSCs, we consider the retention and subsequent growth of seed SMBHs through GW mergers of IMBHs and subsequent gas accretion. Moreover, we check the consequences of these results on the observed demographics of NSCs and the occupation fraction of SMBHs in galaxies.

ACKNOWLEDGEMENTS

We would like to thank the reviewer for a comprehensive report that helped in improving the quality and readability of the manuscript. We would like to thank Long Wang for his assistance in using NBODY6++GPU and to the developers of the code for making it publicly available. AA was supported by the Carl Tryggers Foundation for Scientific Research through the grant CTS 17:113. RC and AA acknowledge support from the Swedish Research Council through the grant 2017-04217. We would like to thank the Royal Physiographic Society of Lund and the Walter Gyllenberg Foundation for the research grant: ‘Evolution of Binaries containing Massive Stars’. Simulations in this project were carried out at LU-NARC, which is the centre for scientific and technical computing at Lund University through the projects LU 2018/2-28, 2019/2-27 and LU 2020/2-14. Simulations were also carried out using the ‘chuck’ computer cluster hosted at the Nicolaus Copernicus Astronomical Centre (CAMK) in Warsaw, Poland.

DATA AVAILABILITY STATEMENT

The simulations in this project were carried out using NBODY6++GPU. The data and output from these simulations will be shared on request to the corresponding author.

REFERENCES

- Aarseth S. J., 1999, *PASP*, **111**, 1333
Aarseth S. J., 2003, *Gravitational N-body simulations: tools and algorithms*. Cambridge University Press
Abbott R., et al., 2020, *ApJ*, **900**, L13
Agarwal M., Milosavljević M., 2011, *ApJ*, **729**, 35
Aharon D., Perets H. B., 2015, *ApJ*, **799**, 185
Ahmad A., Cohen L., 1973, *Journal of Computational Physics*, **12**, 389
Alexander T., Bar-Or B., 2017, *Nature Astronomy*, **1**, 0147
Alister Seguel P. J., Schleicher D. R. G., Boekholt T. C. N., Fellhauer M., Klessen R. S., 2020, *MNRAS*, **493**, 2352
Amaro-Seoane P., Freitag M., 2006, *ApJ*, **653**, L53
Amaro-Seoane P., Gair J. R., Freitag M., Miller M. C., Mandel I., Cutler C. J., Babak S., 2007, *Classical and Quantum Gravity*, **24**, R113
Amaro-Seoane P., et al., 2017, arXiv e-prints, p. arXiv:1702.00786
Antonini F., 2013, *ApJ*, **763**, 62
Antonini F., 2014, *ApJ*, **794**, 106
Antonini F., Capuzzo-Dolcetta R., Mastrobuono-Battisti A., Merritt D., 2012, *ApJ*, **750**, 111
Antonini F., Barausse E., Silk J., 2015, *ApJ*, **812**, 72
Antonini F., Gieles M., Gualandris A., 2019, *MNRAS*, **486**, 5008
Arca-Sedda M., Capuzzo-Dolcetta R., 2014, *MNRAS*, **444**, 3738
Arca-Sedda M., Capuzzo-Dolcetta R., 2017, *MNRAS*, **464**, 3060
Arca-Sedda M., Capuzzo-Dolcetta R., 2019, *MNRAS*, **483**, 152
Arca-Sedda M., Gualandris A., 2018, *MNRAS*, **477**, 4423
Arca Sedda M., Mastrobuono-Battisti A., 2019, arXiv e-prints, p. arXiv:1906.05864
Arca-Sedda M., Capuzzo-Dolcetta R., Antonini F., Seth A., 2015, *ApJ*, **806**, 220
Arca-Sedda M., Capuzzo-Dolcetta R., Spera M., 2016, *MNRAS*, **456**, 2457
Arca Sedda M., Askar A., Giersz M., 2019a, arXiv e-prints, p. arXiv:1905.00902
Arca Sedda M., Berczik P., Capuzzo-Dolcetta R., Fragione G., Sobolenko M., Spurzem R., 2019b, *MNRAS*, **484**, 520
Arca Sedda M., Gualandris A., Do T., Feldmeier-Krause A., Neumayer N., Erkal D., 2020a, arXiv e-prints, p. arXiv:2009.02328
Arca Sedda M., Mapelli M., Spera M., Benacquista M., Giacobbo N., 2020b, *ApJ*, **894**, 133
Aros F. I., Sippel A. C., Mastrobuono-Battisti A., Askar A., Bianchini P., van de Ven G., 2020, *MNRAS*, **499**, 4646
Askar A., Szkudlarek M., Gondek-Rosińska D., Giersz M., Bulik T., 2017, *MNRAS*, **464**, L36
Baker J. G., Boggs W. D., Centrella J., Kelly B. J., McWilliams S. T., Miller M. C., van Meter J. R., 2007, *ApJ*, **668**, 1140
Baker J. G., Boggs W. D., Centrella J., Kelly B. J., McWilliams S. T., Miller M. C., van Meter J. R., 2008, *ApJ*, **682**, L29
Baldassare V. F., Reines A. E., Gallo E., Greene J. E., 2015, *ApJ*, **809**, L14
Baumgardt H., Gualandris A., Portegies Zwart S., 2006, *MNRAS*, **372**, 174
Baumgardt H., et al., 2019, *MNRAS*, **488**, 5340
Berczik P., Merritt D., Spurzem R., 2005, *ApJ*, **633**, 680
Binney J., Tremaine S., 2008, *Galactic Dynamics: Second Edition*. Princeton university press
Blecha L., Cox T. J., Loeb A., Hernquist L., 2011, *MNRAS*, **412**, 2154
Blecha L., et al., 2016, *MNRAS*, **456**, 961
Boekholt T. C. N., Schleicher D. R. G., Fellhauer M., Klessen R. S., Reinoso B., Stutz A. M., Haemmerlé L., 2018, *MNRAS*, **476**, 366
Bonetti M., et al., 2020, *MNRAS*, **493**, L114
Campanelli M., Lousto C., Zlochower Y., Merritt D., 2007, *ApJ*, **659**, L5
Capuzzo-Dolcetta R., 1993, *ApJ*, **415**, 616
Capuzzo-Dolcetta R., Miocchi P., 2008, *ApJ*, **681**, 1136

- Capuzzo-Dolcetta R., Tosta e Melo I., 2017, *MNRAS*, **472**, 4013
- Côté P., et al., 2006, *ApJS*, **165**, 57
- Das A., Schleicher D. R. G., Leigh N. W. C., Boekholt T. C. N., 2020, arXiv e-prints, p. [arXiv:2012.01456](https://arxiv.org/abs/2012.01456)
- Davies M. B., Miller M. C., Bellovary J. M., 2011, *ApJ*, **740**, L42
- Davies M. B., Askar A., Church R. P., 2020, in Bragaglia A., Davies M., Sills A., Vesperini E., eds, IAU Symposium Vol. 351, IAU Symposium. pp 80–83 ([arXiv:1907.13373](https://arxiv.org/abs/1907.13373)), doi:10.1017/S1743921319006689
- Devecchi B., Volonteri M., 2009, *ApJ*, **694**, 302
- Devecchi B., Volonteri M., Rossi E. M., Colpi M., Portegies Zwart S., 2012, *MNRAS*, **421**, 1465
- Di Carlo U. N., Mapelli M., Bouffanais Y., Giacobbo N., Santoliquido F., Bressan A., Spera M., Haardt F., 2020, *MNRAS*, **497**, 1043
- Do T., Martinez G. D., Kerzendorf W., Feldmeier-Krause A., Arca Sedda M., Neumayer N., Gualandris A., 2020, arXiv e-prints, p. [arXiv:2009.02335](https://arxiv.org/abs/2009.02335)
- Dunn G., Holley-Bockelmann K., Bellovary J., 2020, arXiv e-prints, p. [arXiv:2002.04740](https://arxiv.org/abs/2002.04740)
- Ebisuzaki T., et al., 2001, *ApJ*, **562**, L19
- Ferrarese L., et al., 2006, *ApJ*, **644**, L21
- Fitchett M. J., 1983, *MNRAS*, **203**, 1049
- Fragione G., Bromberg O., 2019, *MNRAS*, **488**, 4370
- Fragione G., Silk J., 2020, arXiv e-prints, p. [arXiv:2006.01867](https://arxiv.org/abs/2006.01867)
- Fragione G., Ginsburg I., Kocsis B., 2018a, *ApJ*, **856**, 92
- Fragione G., Leigh N. W. C., Ginsburg I., Kocsis B., 2018b, *ApJ*, **867**, 119
- Fragione G., Loeb A., Rasio F. A., 2020, *ApJ*, **902**, L26
- Freitag M., Gürkan M. A., Rasio F. A., 2006, *MNRAS*, **368**, 141
- Gebhardt K., et al., 2001, *AJ*, **122**, 2469
- Georgiev I. Y., Böker T., Leigh N., Lützgendorf N., Neumayer N., 2016, *MNRAS*, **457**, 2122
- Gerosa D., Berti E., 2019, *Phys. Rev. D*, **100**, 041301
- Gieles M., et al., 2018, *MNRAS*, **478**, 2461
- Giersz M., Heggie D. C., Hurley J. R., Hypki A., 2013, *MNRAS*, **431**, 2184
- Giersz M., Leigh N., Hypki A., Lützgendorf N., Askar A., 2015, *MNRAS*, **454**, 3150
- Gnedin O. Y., Ostriker J. P., Tremaine S., 2014, *ApJ*, **785**, 71
- González J. A., Hannam M., Sperhake U., Brüggmann B., Husa S., 2007, *Phys. Rev. Lett.*, **98**, 231101
- Gordon K. D., Hanson M. M., Clayton G. C., Rieke G. H., Misselt K. A., 1999, *ApJ*, **519**, 165
- Graham A. W., Spitler L. R., 2009, *MNRAS*, **397**, 2148
- Greene J. E., Strader J., Ho L. C., 2019, arXiv e-prints, p. [arXiv:1911.09678](https://arxiv.org/abs/1911.09678)
- Gualandris A., Merritt D., 2012, *ApJ*, **744**, 74
- Guillard N., Emsellem E., Renaud F., 2016, *MNRAS*, **461**, 3620
- Gültekin K., Miller M. C., Hamilton D. P., 2006, *ApJ*, **640**, 156
- Gürkan M. A., Fregeau J. M., Rasio F. A., 2006, *ApJ*, **640**, L39
- Hartmann M., Debattista V. P., Seth A., Cappellari M., Quinn T. R., 2011, *MNRAS*, **418**, 2697
- Haster C.-J., Antonini F., Kalogera V., Mandel I., 2016, *ApJ*, **832**, 192
- Hills J. G., 1983, *AJ*, **88**, 1269
- Hoffman L., Loeb A., 2007, *MNRAS*, **377**, 957
- Holley-Bockelmann K., Gültekin K., Shoemaker D., Yunes N., 2008, *ApJ*, **686**, 829
- Hong J., Askar A., Giersz M., Hypki A., Yoon S.-J., 2020, *MNRAS*, **498**, 4287
- Hurley J. R., Pols O. R., Tout C. A., 2000, *MNRAS*, **315**, 543
- Hurley J. R., Tout C. A., Pols O. R., 2002, *MNRAS*, **329**, 897
- Hypki A., Giersz M., 2013, *MNRAS*, **429**, 1221
- Inayoshi K., Haiman Z., Ostriker J. P., 2016, *MNRAS*, **459**, 3738
- Iwasawa M., An S., Matsubayashi T., Funato Y., Makino J., 2011, *ApJ*, **731**, L9
- Johnson J. L., Whalen D. J., Li H., Holz D. E., 2013, *ApJ*, **771**, 116
- Khan F. M., Berentzen I., Berczik P., Just A., Mayer L., Nitadori K., Callegari S., 2012, *ApJ*, **756**, 30
- Khan F. M., Holley-Bockelmann K., Berczik P., Just A., 2013, *ApJ*, **773**, 100
- Khan F. M., Capelo P. R., Mayer L., Berczik P., 2018, *ApJ*, **868**, 97
- Khan F. M., Mirza M. A., Holley-Bockelmann K., 2020, *MNRAS*, **492**, 256
- Kim S. S., Figer D. F., Morris M., 2004, *ApJ*, **607**, L123
- King A. R., Pringle J. E., 2006, *MNRAS*, **373**, L90
- King A. R., Pringle J. E., Hofmann J. A., 2008, *MNRAS*, **385**, 1621
- Kızıltan B., Baumgardt H., Loeb A., 2017, *Nature*, **542**, 203
- Kormendy J., McClure R. D., 1993, *AJ*, **105**, 1793
- Kremer K., et al., 2020, *ApJ*, **903**, 45
- Kroupa P., 2001, *MNRAS*, **322**, 231
- Kustaanheimo P., Stiefel E., 1965, *J. Reine Angew. Math.*, **218**, 204
- Lanzoni B., et al., 2013, *ApJ*, **769**, 107
- Latif M. A., Ferrara A., 2016, *Publ. Astron. Soc. Australia*, **33**, e051
- Lee M. H., 1993, *ApJ*, **418**, 147
- Leigh N. W. C., Böker T., Maccarone T. J., Perets H. B., 2013, *MNRAS*, **429**, 2997
- Leigh N. W. C., Lützgendorf N., Geller A. M., Maccarone T. J., Heinke C., Sesana A., 2014, *MNRAS*, **444**, 29
- Leigh N. W. C., Georgiev I. Y., Böker T., Knigge C., den Brok M., 2015, *MNRAS*, **451**, 859
- Lin D., et al., 2018, *Nature Astronomy*, **2**, 656
- Lin D., et al., 2020, *ApJ*, **892**, L25
- Loose H. H., Kruegel E., Tutukov A., 1982, *A&A*, **105**, 342
- Lotz J. M., Telford R., Ferguson H. C., Miller B. W., Stiavelli M., Mack J., 2001, *ApJ*, **552**, 572
- Lousto C. O., Zlochower Y., 2008, *Phys. Rev. D*, **77**, 044028
- Lousto C. O., Zlochower Y., Dotti M., Volonteri M., 2012, *Phys. Rev. D*, **85**, 084015
- Lützgendorf N., et al., 2013a, *A&A*, **552**, A49
- Lützgendorf N., Baumgardt H., Kruijssen J. M. D., 2013b, *A&A*, **558**, A117
- MacLeod M., Guillochon J., Ramirez-Ruiz E., Kasen D., Rosswog S., 2016, *ApJ*, **819**, 3
- Madau P., Haardt F., Dotti M., 2014, *ApJ*, **784**, L38
- Makino J., Funato Y., 2004, *ApJ*, **602**, 93
- Mann C. R., et al., 2019, *ApJ*, **875**, 1
- Mapelli M., 2016, *MNRAS*, **459**, 3432
- Martinez M. A. S., et al., 2020, *ApJ*, **903**, 67
- Mastrobuono-Battisti A., Perets H. B., Loeb A., 2014, *ApJ*, **796**, 40
- Mastrobuono-Battisti A., Khoperskov S., Di Matteo P., Haywood M., 2019, *A&A*, **622**, A86
- Mayer L., Kazantzidis S., Escala A., Callegari S., 2010, *Nature*, **466**, 1082
- Merritt D., 2006, *ApJ*, **648**, 976
- Merritt D., Ferrarese L., Joseph C. L., 2001, *Science*, **293**, 1116
- Merritt D., Milosavljević M., Favata M., Hughes S. A., Holz D. E., 2004, *ApJ*, **607**, L9
- Mezcua M., 2017, *International Journal of Modern Physics D*, **26**, 1730021
- Mihos J. C., Hernquist L., 1994, *ApJ*, **437**, L47
- Mikkola S., Aarseth S. J., 1993, *Celestial Mechanics and Dynamical Astronomy*, **57**, 439
- Miller M. C., Davies M. B., 2012, *ApJ*, **755**, 81
- Miller M. C., Hamilton D. P., 2002, *MNRAS*, **330**, 232
- Milosavljević M., 2004, *ApJ*, **605**, L13
- Miocchi P., Capuzzo Dolcetta R., Di Matteo P., Vicari A., 2006, *ApJ*, **644**, 940
- Morawski J., Giersz M., Askar A., Belczynski K., 2018, *MNRAS*, **481**, 2168
- Nasim I., Gualandris A., Read J., Dehnen W., Delorme M., Antonini F., 2020, *MNRAS*, **497**, 739
- Natarajan P., 2020, arXiv e-prints, p. [arXiv:2009.09156](https://arxiv.org/abs/2009.09156)
- Nayakshin S., Cuadra J., Springel V., 2007, *MNRAS*, **379**, 21
- Neumayer N., Walcher C. J., 2012, *Advances in Astronomy*, **2012**, 709038
- Neumayer N., Seth A., Boeker T., 2020, arXiv e-prints, p. [arXiv:2001.03626](https://arxiv.org/abs/2001.03626)
- Nguyen D. D., Seth A. C., Reines A. E., den Brok M., Sand D., McLeod B., 2014, *ApJ*, **794**, 34
- Nguyen D. D., et al., 2019, *ApJ*, **872**, 104
- Nitadori K., Aarseth S. J., 2012, *MNRAS*, **424**, 545
- Noyola E., Gebhardt K., Bergmann M., 2008, *ApJ*, **676**, 1008
- Ogiya G., Hahn O., Mingarelli C. M. F., Volonteri M., 2020, *MNRAS*, **493**, 3676
- Oh K. S., Lin D. N. C., 2000, *ApJ*, **543**, 620
- Pacucci F., Natarajan P., Volonteri M., Cappelluti N., Urry C. M., 2017, *ApJ*, **850**, L42

Panamarev T., Just A., Spurzem R., Berczik P., Wang L., Arca Sedda M., 2019, *MNRAS*, **484**, 3279

Pechetti R., Seth A., Neumayer N., Georgiev I., Kacharov N., den Brok M., 2020, *ApJ*, **900**, 32

Peters P. C., 1964, *Phys. Rev.*, **136**, B1224

Petts J. A., Gualandris A., 2017, *MNRAS*, **467**, 3775

Portegies Zwart S. F., McMillan S. L. W., 2002, *ApJ*, **576**, 899

Portegies Zwart S. F., Baumgardt H., McMillan S. L. W., Makino J., Hut P., Ebisuzaki T., 2006, *ApJ*, **641**, 319

Quinlan G. D., 1996, *New Astron.*, **1**, 35

Quinlan G. D., Shapiro S. L., 1990, *ApJ*, **356**, 483

Rasskazov A., Fragione G., Kocsis B., 2019, arXiv e-prints, p. [arXiv:1912.07681](https://arxiv.org/abs/1912.07681)

Rastello S., Amaro-Seoane P., Arca-Sedda M., Capuzzo-Dolcetta R., Fragione G., Tosta e Melo I., 2019, *MNRAS*, **483**, 1233

Reinoso B., Schleicher D. R. G., Fellhauer M., Klessen R. S., Boekholt T. C. N., 2018, *A&A*, **614**, A14

Rizzuto F. P., et al., 2020, arXiv e-prints, p. [arXiv:2008.09571](https://arxiv.org/abs/2008.09571)

Rodríguez C. L., Zevin M., Amaro-Seoane P., Chatterjee S., Kremer K., Rasio F. A., Ye C. S., 2019, *Phys. Rev. D*, **100**, 043027

Romero-Shaw I., Lasky P. D., Thrane E., Calderón Bustillo J., 2020, *ApJ*, **903**, L5

Rossow S., Ramirez-Ruiz E., Hix W. R., 2009, *ApJ*, **695**, 404

Sakurai Y., Yoshida N., Fujii M. S., Hirano S., 2017, *MNRAS*, **472**, 1677

Sakurai Y., Yoshida N., Fujii M. S., 2019, *MNRAS*, **484**, 4665

Samsing J., 2018, *Phys. Rev. D*, **97**, 103014

Samsing J., Hotokezaka K., 2020, arXiv e-prints, p. [arXiv:2006.09744](https://arxiv.org/abs/2006.09744)

Schödel R., Gallego-Cano E., Dong H., Noguera-Lara F., Gallego-Calvente A. T., Amaro-Seoane P., Baumgardt H., 2018, *A&A*, **609**, A27

Sesana A., 2010, *ApJ*, **719**, 851

Sesana A., Haardt F., Madau P., 2006, *ApJ*, **651**, 392

Seth A., Agüeros M., Lee D., Basu-Zych A., 2008, *ApJ*, **678**, 116

Seth A. C., Neumayer N., Böker T., 2020, in Bragaglia A., Davies M., Sills A., Vesperini E., eds, IAU Symposium Vol. 351, IAU Symposium. pp 13–18 ([arXiv:1908.00022](https://arxiv.org/abs/1908.00022)), doi:[10.1017/S1743921319007117](https://doi.org/10.1017/S1743921319007117)

Stone N. C., Küpper A. H. W., Ostriker J. P., 2017, *MNRAS*, **467**, 4180

Strader J., Chomiuk L., Maccarone T. J., Miller-Jones J. C. A., Seth A. C., Heinke C. O., Sivakoff G. R., 2012, *ApJ*, **750**, L27

Tagawa H., Haiman Z., Kocsis B., 2020, *ApJ*, **892**, 36

Takekawa S., Oka T., Iwata Y., Tsujimoto S., Nomura M., 2019, *ApJ*, **871**, L1

Takekawa S., Oka T., Iwata Y., Tsujimoto S., Nomura M., 2020, *ApJ*, **890**, 167

Tamfal T., Capelo P. R., Kazantzidis S., Mayer L., Potter D., Stadel J., Widrow L. M., 2018, *ApJ*, **864**, L19

Tremaine S. D., Ostriker J. P., Spitzer L. J., 1975, *ApJ*, **196**, 407

Tremou E., et al., 2018, *ApJ*, **862**, 16

Tsatsi A., Mastrobuono-Battisti A., van de Ven G., Perets H. B., Bianchini P., Neumayer N., 2017, *MNRAS*, **464**, 3720

Vesperini E., McMillan S. L. W., D’Ercole A., D’Antona F., 2010, *ApJ*, **713**, L41

Volonteri M., 2007, *ApJ*, **663**, L5

Volonteri M., 2010, *A&ARv*, **18**, 279

Wang L., Berczik P., Spurzem R., Kouwenhoven M. B. N., 2014, *ApJ*, **780**, 164

Wang L., Spurzem R., Aarseth S., Nitadori K., Berczik P., Kouwenhoven M. B. N., Naab T., 2015, *MNRAS*, **450**, 4070

Wirth H., Bekki K., 2020, arXiv e-prints, p. [arXiv:2006.02517](https://arxiv.org/abs/2006.02517)

Wiseman A. G., 1992, *Phys. Rev. D*, **46**, 1517

Zocchi A., Gieles M., Hénault-Brunet V., 2019, *MNRAS*, **482**, 4713

de Vita R., Trenti M., Bianchini P., Askar A., Giersz M., van de Ven G., 2017, *MNRAS*, **467**, 4057

de Vita R., Trenti M., MacLeod M., 2018, *MNRAS*, **475**, 1574

van Meter J. R., Miller M. C., Baker J. G., Boggs W. D., Kelly B. J., 2010, *ApJ*, **719**, 1427

APPENDIX A: DYNAMICALLY-DRIVEN EVOLUTION OF BINARY IMBHs

A binary IMBH in one of our simulations forms at moderate to high eccentricities, immersed in a sea of lower-mass stars. As it interacts with those stars it loses energy and the binary’s orbit hardens, but it also either becomes more eccentric or maintains a high eccentricity (see Fig. 7). Other authors have observed this phenomenon of eccentricity-pumping; e.g. Amaro-Seoane & Freitag (2006); Arca Sedda & Mastrobuono-Battisti (2019) in IMBH binaries, Rastello et al. (2019) in stellar mass BH binaries and Sesana (2010); Iwasawa et al. (2011); Khan et al. (2012); Ogiya et al. (2020); Bonetti et al. (2020) in SMBH binaries. In each case the distinguishing feature is that the bodies that make up the binary are more massive than the bodies with which the binary is interacting. We investigated to see whether this is a general effect.

Our binaries are, at least initially, too wide for general relativistic effects to play a significant role in their orbital evolution. Hence changes of semi-major axis a and eccentricity e are driven by interactions with stars. Such interactions can be with the smooth potential arising from the combined effects of many stars; alternatively, strong scatterings with individual stars can also change the binary’s orbit. It is the second effect that we consider here.

The binary IMBH that we form is, within a short time frame, dynamically hard (strongly bound). This means that it cannot be disrupted by an encounter with an individual star, and that the net effect of encounters is to harden the binary further. It is convenient to analyse the effect on the binary orbit by considering the interaction between one of the two IMBHs and a star. These encounters systematically act in the opposite direction to the relative motion of the star and the IMBH. Since the binary orbital velocity $v_{\text{orb}} \gtrsim \sigma$, where σ is the stellar velocity dispersion, this, on average, slows the IMBH along its original direction of motion. It also imparts a small additional momentum in a direction perpendicular to the IMBH’s original direction of motion, the plane of which depends on the initial velocity of the incoming star.

We consider for now solely the braking component of the encounter and analyse its effect on the orbit at pericentre and apocentre. At pericentre, slowing the motion of one of the stars does not affect the pericentre separation, $r_{\text{peri}} = a(1 - e)$, since the resulting orbit is closed, but decreases a . Hence braking encounters at pericentre circularise an orbit, as seen in, for example, the effects of tides on binary star orbits. Conversely, braking encounters at apocentre do not change the apocentre separation, $r_{\text{apo}} = a(1 + e)$, but decrease the semi-major axis. This drives the orbit to higher eccentricities. This means that for purely braking encounters, the ratio of the rate of encounters around pericentre to that around apocentre will determine whether the orbit is driven to lower or higher eccentricities. For a binary embedded at the centre of a uniform-density sea of low-mass particles, as in Chandrasekhar’s derivation of dynamical friction, the binary spends longer time at apocentre than pericentre, and hence more encounters happen at apocentre. Hence as long as a is smaller than the scale on which the stellar density changes we would expect encounters with low-mass stars to drive the binary to higher eccentricities.

However, as Fig. 6 shows, this is not an appropriate description of the physical scenario in which our binaries find themselves. After a short space of time they have scattered out all the stars within their orbits. Further orbital evolution is driven by stochastic encounters with stars that are scattered in from outside. Hence we construct a toy model of these scatterings to investigate whether it behaves like our N -body simulations. We draw stars from the

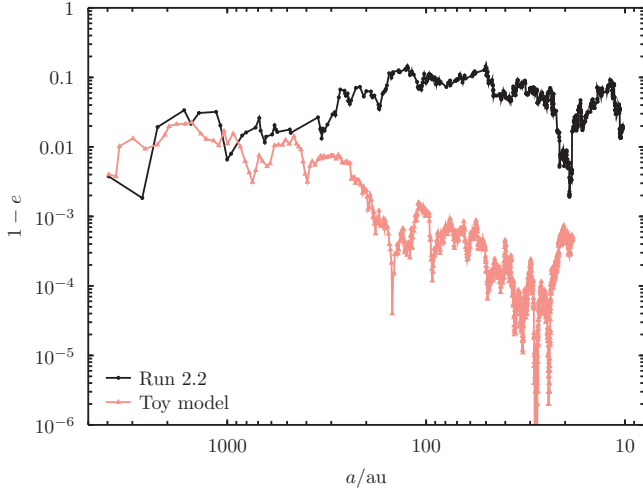


Figure A1. Comparison of toy model with N -body model. The plot shows the semi-major axis a vs $1 - e$ up to a time of 763 Myr, starting when the binary formed. The black line shows results from the N -body model for binary 2.2 and the pink line shows the results from the toy model.

same mass function as in our simulations, a power-law with index $\gamma = -2.3$ between $0.5 M_{\odot}$ and $2 M_{\odot}$. Following an inspection of the kinematic properties of the stars within 0.1 pc of the central binary in our N -body models, we take the stars to have a mass density $\rho = 10^4 M_{\odot} \text{pc}^{-3}$. Their velocities follow a Maxwellian distribution with $\sigma = 15 \text{ km s}^{-1}$. We choose impact parameters b distributed uniformly in b^2 up to $b_{\text{max}} \equiv \tilde{b}_{\text{max}} a$ with $\tilde{b}_{\text{max}} = 100$. The time between encounters is exponentially distributed with a mean interval of

$$\bar{\Delta t} = \frac{1}{n\sigma\pi\tilde{b}_{\text{max}}^2 a^2}. \quad (\text{A1})$$

We consider encounters between the star and one of the two BHs, chosen at random. For each encounter we choose a uniformly distributed mean anomaly for the central binary and solve the Kepler problem to obtain the position of our chosen IMBH in the binary centre of mass frame. The encounter between the star of mass m and the IMBH of mass M acts to change the velocity of the IMBH parallel and perpendicular to the relative velocity of the IMBH and star following (Binney & Tremaine 2008, eq. 3.54)

$$|\Delta \mathbf{v}_{M\perp}| = \frac{2mV_0}{M+m} \frac{b/b_{90}}{1 + (b/b_{90})^2} \quad (\text{A2})$$

and

$$|\Delta \mathbf{v}_{M\parallel}| = \frac{2mV_0}{M+m} \frac{1}{1 + (b/b_{90})^2} \quad (\text{A3})$$

where the relative velocity is V_0 and

$$b_{90} = \frac{G(M+m)}{V_0^2}. \quad (\text{A4})$$

position of IMBH in binary COM frame.

Since the stars should approach the binary with isotropically distributed velocity vectors we pick a perpendicular direction uniformly distributed on a circle. We then apply the effects of the encounter to the IMBH's velocity vector, recompute the orbital elements of the binary, and repeat.

The resulting evolution of the orbital elements for our model

of run 2.2 are shown in Fig. A1. The model qualitatively captures some of the key features of the evolution. In roughly the correct time span the binary is driven together, with the orbital semi-major axis shrinking by a factor of about 300. At the same time the binary is maintained at very high eccentricities, but the eccentricity fluctuates considerably as the IMBH, almost stationary at apocentre, is buffeted by the incoming stars. There are two deficiencies to the toy model. The eccentricity is still driven to higher values than in the N -body run, and the orbit does not shrink enough. Both of these differences can be attributed to only considering the effect of the encounters on one of the IMBHs at a time. In reality, weak encounters at large impact parameters torque both stars, systematically removing more energy from the binary and reducing the impact on the eccentricity, since the two IMBHs will be scattered in roughly the same direction. However, the degree of qualitative agreement that we do see in Fig. A1 confirms that the eccentricity pumping is a physical effect owing to the processes that we describe and not a manifestation of numerical problems in the N -body code. Additionally, in the N -body model the binary is free to move, compared to the toy model. This implies that the binary recoils in scattering events, thus part of the energy transfer is absorbed by the binary motion rather than being fully dissipated into the scattered star. As a result the binary hardening is less effective in the simulated run as compared to the toy model.

This paper has been typeset from a \LaTeX file prepared by the author.